AGU PUBLICATIONS

JGR

Journal of Geophysical Research: Atmospheres

RESEARCH ARTICLE
10.1002/2016JD024858

Key Points:
- Deficiencies are found in the estimation of drought severity, spatial pattern, and temporal persistency of droughts by reanalyses
- Differences are attributed to high monthly to seasonal precipitation variability
- Wet bias further increases after approximately 1999 due to changes in the observations included in the reanalyses assimilation systems

Correspondence to:
W. Zhan,
wzhan@princeton.edu

Citation:
Zhan, W., K. Guan, J. Sheffield, and E. F. Wood (2016), Depiction of drought over sub-Saharan Africa using reanalyses precipitation data sets, *J. Geophys. Res. Atmos.*, *121*, 10,555–10,574, doi:10.1002/2016JD024858.

Received 11 FEB 2016
Accepted 28 AUG 2016
Accepted article online 6 SEP 2016
Published online 24 SEP 2016

Depiction of drought over sub-Saharan Africa using reanalyses precipitation data sets

Wang Zhan[1], Kaiyu Guan[2], Justin Sheffield[1], and Eric F. Wood[1]

[1]Department of Civil and Environmental Engineering, Princeton University, Princeton, New Jersey, USA, [2]Department of Natural Resources and Environmental Science, University of Illinois at Urbana-Champaign, Urbana, Illinois, USA

Abstract Reanalysis precipitation is routinely used as a surrogate for observations due to its high spatial and temporal resolution and global coverage, and it has been widely used in hydrologic and agricultural applications. The resultant product and analysis are largely dependent on the accuracy of the reanalysis precipitation data set. In this study, we analyze the impact of reanalysis precipitation uncertainties on drought depiction. Five reanalyses precipitation data sets (Climate Forecast System Reanalysis, R1: National Centers for Environmental Prediction (NCEP)/National Center for Atmospheric Research reanalysis, R2: NCEP/Department of Energy reanalysis II, 20CR: The Twentieth Century Reanalysis version 2 and Modern-Era Retrospective Analysis for Research and Applications) are evaluated from 1979 to 2012 over sub-Saharan Africa against an observational-based reference: The Princeton Global Meteorological Forcing data set. Results show that all the reanalyses precipitation data sets provide a relatively good representation of the long-term statistics of spatiotemporal drought characteristics in sub-Saharan Africa. However, deficiencies are found in the estimation of drought severity, the spatial pattern, and temporal persistency of droughts. Drought depiction over central Africa appears more problematic due to a lack of observational data. A comparison of drought depiction based on the Standardized Precipitation Index reveals higher monthly to seasonal precipitation variability that further increases after ~1999 due to changes in the observations included in the reanalyses assimilation systems.

1. Introduction

Drought accounts for widespread agricultural failure and famine and threats future water and food supplies as well as to regional economies. It is estimated that in the twentieth century, nearly 1.9 billion people have been affected by drought [*Sheffield et al*., 2012]. However, the dynamics of tropical drought onset, persistence, and recovery are one of the least understood aspects of this natural disaster. As a critical characteristic of the hydrologic cycle, drought is primarily caused by a precipitation deficit and propagates through the hydrologic cycle affecting all components. Thus, knowledge about precipitation amounts and their patterns are crucial for understanding drought mechanisms, monitoring current drought conditions, predicting future drought risks, and mitigating potential impacts on agriculture and water availability.

Valuable ground-based precipitation records that can be used for drought monitoring or prediction are often lacking, especially in developing countries where precipitation networks are sparse. Precipitation reanalyses data generated from state-of-the-art global circulation models, with assimilation of multiple-source satellite or observational data, bring substantial opportunities to the hydrologic and climate community. Reanalysis has been increasingly used as a surrogate of observations in long-term monitoring of water-driven processes such as climate predictions and drought monitoring [*Mo and Chelliah*, 2006; *Dutra et al*., 2008]. By merging available observations with a climate model, reanalysis offers valuable information, especially over poorly monitored regions such as sub-Saharan Africa.

However, substantial uncertainty exists in hydrological variables in reanalyses data sets, especially in tropical regions, which may lead to an unrealistic representation of the water cycle variables [*Lorenz and Kunstmann*, 2012; *Zhang et al*., 2013]. Precipitation, being one of the key components of the water and energy cycles, is particularly important since its accuracy, to a large extent, determines the reliability of hydrological model outputs. A number of studies have been carried out on the evaluation of reanalyses-based precipitation at regional [e.g., *Koutsouris et al*., 2015], continental [e.g., *Solman et al*., 2013; *Peña-Arancibia et al*., 2013] and global scales [e.g., *Betts et al*., 2006, 2009; *Bosilovich et al*., 2008]. The reanalyses data sets have been found to suffer from a lack of closure of the water budget over the tropics [*Marengo*, 2005] and have failed in

reproducing the increasing tendency of the North African monsoon precipitation [*Lin et al*., 2014]. Intercomparison studies have demonstrated major differences in the tropical regions between reanalyses precipitation and observations [*Lorenz and Kunstmann*, 2012; *Zhang et al*., 2013]. Some differences have been attributed to the misrepresentation of rain rate distribution [*Rienecker et al*., 2011] as well as biases in rainfall climatology and variability [*Poccard et al*., 2000].

Errors in reanalyses products are associated with parameterizations in the physical processes and the data assimilation procedures [*Zhang et al*., 2012], leading to uncertainties when they are used to force hydrological models and other applications like crop models. A few of the evaluation studies focused on assessing and understanding the impact of errors in reanalyses data sets on hydrological modeling [e.g., *Adler et al*., 2001; *Solman et al*., 2013]. Precipitation has been demonstrated to be a significant source of uncertainty in simulated runoff on different time scales from daily [*Getirana et al*., 2011] to decadal [*Fekete et al*., 2004].

Quantitative assessment of drought characteristics and the impact of historical drought events are essential for managing water resources, irrigation planning, and food security. For this purpose, several indices have been derived in recent years to quantify different drought parameters, such as its intensity, duration, frequency, and severity. *Mishra and Singh* [2010] and *Dai* [2011] gave comprehensive reviews on drought indexes commonly used, and newly developed, for different types of drought. One of the most frequently used drought indices to characterize meteorological drought is the Standardized Precipitation Index (SPI) [*McKee et al*., 1993]. SPI is a normalized index representing the standardized departure of an observed rainfall amount compared to long-term rainfall climatology. It is recommended by the World Meteorological Organization to monitor the severity of drought events. *Sheffield et al*. [2004] developed a drought index based on soil moisture percentiles (Q_{SM}) derived from a 50 year, historical soil moisture time series from the Variable Infiltration Capacity (VIC) land surface model. This soil moisture-based drought index was first used over the continental U.S. and has been adopted by the North American Land Data Assimilation System to represent drought severities and durations over the U.S. and is used in Princeton's African Flood and Drought Monitor [*Sheffield et al*., 2014].

As a dynamic process, it is important to investigate spatial-temporal patterns of drought. Efforts have been made to relate different aspects of drought characteristics [*Hallack-Alegria and Watkins*, 2007; *Mishra and Singh*, 2009]. Among the others is the innovative severity-area-duration (SAD) analysis developed by *Andreadis et al*. [2005], which quantifies relationships between drought severity, spatial extent, and duration in an objective manner. The novelty of the SAD analysis lies in integrating the spatiotemporal information without reducing events to a lower dimension. SAD analysis has been successfully used to compare agricultural drought events over the continental United States [*Wang et al*., 2009], Korea [*Kim et al*., 2011], China [*Wang et al*., 2011], and globally [*Sheffield et al*., 2009] using soil moisture percentiles.

In this study, we evaluate five reanalyses precipitation data sets on their reconstruction of drought properties over sub-Saharan Africa by implementing the SAD procedure outlined in *Andreadis et al*. [2005]. SAD analysis is applied to track Q_{SM}- and SPI-based drought events over the period 1979 to 2012 and to determine the variability among the reanalyses products in depicting such droughts. The five reanalyses products used in the study are as follows: (i) Climate Forecast System Reanalysis (CFSR) [*Saha et al*., 2010], (ii) National Centers for Environmental Prediction/National Center for Atmospheric Research (NCEP/NCAR) reanalysis (R1) [*Kalnay et al*., 1996], (iii) NCEP/Department of Energy (DOE) reanalysis (R2) [*Kanamitsu et al*., 2002], (iv) twentieth century reanalysis (20CR) [*Compo et al*., 2011], and (v) Modern-Era Retrospective Analysis for Research and Applications (MERRA) [*Rienecker et al*., 2011]. The observational reference used for comparison with the reanalyses is the Princeton Global Forcing data set (PGF) [*Sheffield et al*., 2006]. The assessment is based on simulated soil moisture at a 0.5° spatial resolution from macroscale land surface model, Variable Infiltration Capacity (VIC) model (version 4.1.2, in full water and energy balance mode), driven by observed meteorological data, and the five reanalyses precipitation data sets.

2. Data Sets

Here we compare the precipitation fields from five state-of-the-art reanalyses data sets to the observational precipitation reference from the PGF data set. The five reanalyses data sets mentioned in the previous section are further summarized in Table 1 and briefly described in section 2.1. The PGF precipitation and other forcing data used to run the VIC land surface model are described in more detail in section 2.2. All data are

Table 1. Summary of Reanalysis Precipitation Data Sets Evaluated

Data Set	Assimilation	Temporal Coverage	Spatial Coverage	Model Resolution	Source	Reference
CFSR	3D-VAR	1979/01 to present, 6-hourly	Global, 0.5° × 0.5°	T382 Gaussian grid	NCEP	*Saha et al.* [2010]
R1	3D-VAR	1948/01 to present, 6-hourly	Global, 2.5° × 2.5°	T62 Gaussian grid	NCEP/NCAR	*Kalnay et al.* [1996]
R2	3D-VAR	1979/01 to present, 6-hourly	Global, 2.5° × 2.5°	T62 Gaussian grid	NCEP/DOE	*Kanamitsu et al.* [2002]
20CR	EnKF	1871/01–2012/12, 6-hourly	Global, T62 Gaussian grid	T62 Gaussian grid	NOAA	*Compo et al.* [2011]
MERRA	3D-VAR[a]	1979/01 to present, 1 hourly	Global, 0.5° × 0.667°	0.5° × 0.667°	NASA	*Rienecker et al.* [2011]

[a]With incremental update.

interpolated onto a 0.5° × 0.5° grid using a bilinear interpolation technique. We acknowledge that there are uncertainties introduced by the interpolation since different reanalyses have different spatial resolution. The reanalyses data was aggregated to monthly values for the analysis and covers the period 1979 to 2012.

2.1. Reanalyses Precipitation Data

This section briefly describes the reanalyses from which the precipitation products were derived.

2.1.1. Climate Forecast System Reanalysis (CFSR)

The NCEP CFSR [*Saha et al.*, 2010] covers the period from 1979 to present with a spatial resolution of T382 (~38 km). It includes a coupled atmosphere-ocean model consisting of a spectral atmospheric model from the NCEP Global Forecast System (GFS) [*Saha et al.*, 2006] and an ocean component from the Geophysical Fluid Dynamics Laboratory Modular Ocean Model version 4p0d [*Griffies et al.*, 2004]. Also included is the Global Land Data Assimilation System (GLDAS) Land Information System (LIS) using observed precipitation with a four-layered Noah land surface model (LSM) [*Ek et al.*, 2003], as well as the atmospheric grid-point statistical interpolation (GSI) data assimilation system [*Wu et al.*, 2002]. Precipitation observations from the 5 day satellite-based Climate Prediction Center (CPC) Merged Analysis of Precipitation (CMAP) [*Xie and Arkin*, 1997] with 2.5° × 2.5° spatial resolution and CPC unified global gauge analysis [*Xie et al.*, 2007; *Chen et al.*, 2008] with 0.5° × 0.5° spatial resolution are used as direct forcing to the GLDAS land surface analysis [*Meng et al.*, 2012].

2.1.2. NCEP/NCAR Reanalysis (R1)

The NCEP/NCAR reanalysis system [*Kalnay et al.*, 1996] includes the NCEP Global Spectral Model (GSM, also referred to as the Medium Range Forecast model) with T62 (~210 km) horizontal resolution and a three-dimensional variational (3D-Var) assimilation scheme. The NCEP GSM became operational in January 1995 and is based on the 1988 version of the model (National Meteorological Center Development Division, 1988) with improvements summarized by *Kanamitsu* [1989] and *Kanamitsu et al.* [1991]. Observational data used in the assimilation system [*Kistler et al.*, 1994] include radiosonde observations, Advanced Television Infrared Observation Satellite (TIROS-N) Operational Vertical Sounder temperature soundings, cloud-tracked winds from geostationary satellite, aircraft observations of wind and temperature, land surface reports of surface pressure, ocean reports of surface pressure, temperature, horizontal wind, and specific humidity. Observed precipitation is not included in the assimilation phase of the model. The daily NCEP/NCAR reanalysis precipitation fields, available from 1948 to the present, are averaged from 6-hourly model forecasts (0000 UTC, 0600 UTC, 1200 UTC, and 1800 UTC) and then aggregated to monthly precipitation.

2.1.3. NCEP/DOE Reanalysis II (R2)

The NCEP/Department of Energy (DOE) Atmospheric Modelling Intercomparison Project 2 reanalysis (R2) [*Kanamitsu et al.*, 2002] followed the NCEP/NCAR Reanalysis Project with an updated forecast model (1999 version of NCEP GSM), data assimilation system, and improved physical parameterization. The most significant changes in R2 that directly affect the precipitation forecasts are improved convective parameterization and the incorporation of precipitation observations instead of analysis precipitation to compute soil moisture within a GLDAS system [*Kanamitsu et al.*, 2002]. The observed precipitation database used is the 5 day accumulated Xie-Arkin precipitation [*Xie and Arkin*, 1997], which is a global data set based on both gauge and satellite estimates. Thus, an improved representation of precipitation and soil moisture variability is found in R2 [*Roads*, 2003; *Maurer et al.*, 2001]. Data from NCEP/DOE Reanalysis II are available from January 1979 to the present with T62 (~210 km) horizontal resolution, and this study uses the monthly precipitation fields (aggregated from 6-hourly to monthly) from 1979 to 2012.

2.1.4. The Twentieth Century Reanalysis v2 (20CR)

The Twentieth Century Reanalysis (20CR) [*Compo et al*., 2011] project is an international effort to produce a comprehensive global atmospheric circulation data set spanning the twentieth century. The system is driven by global sea surface temperature and sea ice distributions from the Hadley centre global sea ice and sea surface temperature data set as boundary conditions. The unique feature of 20CR is that it assimilates only surface level pressure records into the coupled atmosphere-land model, which is the April 2008 experimental version of the NCEP GFS, using an Ensemble Kalman Filter (EnKF) data assimilation method [*Whitaker et al*., 2004]. This unique feature allows it to span over a longer time period from 1871 to 2012 and is available at 6-hourly temporal resolution at a $2° \times 2°$ spatial resolution.

2.1.5. Modern-Era Retrospective Analysis for Research and Applications (MERRA)

NASA Goddard Space Flight Center Global Modeling and Assimilation Office conducted the MERRA reanalysis [*Rienecker et al*., 2011]. MERRA reanalysis surface products are available for the period of 1979 to the present, at high spatial and temporal resolution: $0.5° \times 0.667°$ and hourly, respectively. It is based on NASA's Goddard Earth Observing System version 5 (GEOS-5) [*Rienecker et al*., 2008] that includes the GEOS-5 global climate model with observed sea surface temperatures and the Catchment land surface scheme [*Koster et al*., 2000]. The data assimilation used is the NCEP GSI system, a three-dimensional variational (3D-Var) data assimilation system developed by NCEP [*Wu et al*., 2002]. MERRA assimilates satellite rainfall estimates from the Special Sensor Microwave Imager (SSM/I) and the Tropical Rainfall Measuring Mission (TRMM) Microwave Imager (TMI).

2.2. Gridded Observation and Other Forcing Data

The observational reference precipitation data set and other meteorological forcings are taken from the Princeton Global Meteorological Forcing data set (PGF) [*Sheffield et al*., 2006], which has a resolution of 3-hourly and 1° spatially of near-surface meteorology for global land areas for the period 1948–2010. PGF offers multiple variables that can be used to drive land surface models including precipitation, temperature, pressure, downward shortwave and longwave radiation, specific humidity, and wind speed. The precipitation field merges R1 with observations from the 1° Global Precipitation Climatology Project (GPCP) [*Huffman et al*., 2001] daily precipitation, the 0.5° Climatic Research Unit [*New et al*., 2000; *Harris et al*., 2014] monthly values and a 2° gauge-based daily precipitation data set developed by *Nijssen et al*. [2001]. The 0.25° TRMM Multi-Satellite Precipitation Analysis [*Huffman et al*., 2007] 3-hourly real-time data set (3B42RT) is used to downscale precipitation data from 2°, daily to 1°, 3-hourly over the TRMM domain region. The data set has been extensively used in regional and global studies of climate and hydrology applications [*Sheffield and Wood*, 2008; *Wang et al*., 2011]. Given a lack of available high-quality observations for Africa, it is believed that PGF provides the most reliable information about precipitation climatology and variability over Africa under current conditions, despite its inevitable uncertainties [*Chaney et al*., 2014]. Thus, this data set is used as the reference data set in our study.

3. Materials and Methods

3.1. Variable Infiltration Capacity (VIC) Model

The Variable Infiltration Capacity (VIC) model [*Liang et al*., 1994] is used to dynamically simulate the hydrological response of the surface water budget components—namely, surface and subsurface runoff, evapotranspiration, and changes in soil moisture—to atmospheric forcings. A three-layer-soil-moisture representation is simulated through a soil-vegetation-atmosphere transfer [*Liang et al*., 1996] scheme that accounts for subgrid-scale heterogeneity of vegetation, soil, and topography. The VIC simulated water budget components, and particularly runoff and soil moisture, has been validated extensively over the globe to observations [e.g., *Sheffield et al*., 2004]. *Nijssen et al*. [2001] compared monthly soil moisture patterns from VIC simulations to a climatology of soil moisture values by *Mintz and Serafini* [1992]. They conclude that VIC simulated patterns of soil moisture storage mirrors those of *Mintz and Serafini* [1992], with the exception of high-latitude regions in the summer time. The model is run either in full energy mode at a subdaily time step and forced by precipitation, surface incoming shortwave and longwave radiation, and surface meteorology or run in water balance mode at a daily time step and forced with daily precipitation and maximum and minimum air temperatures. In this study, VIC was run in daily water balance mode at a 0.5° spatial resolution, with a spin-up period from 1 January 1970 to 31 December 1978 using PGF precipitation and temperature data.

3.2. Drought Indexes

The simulated soil moisture fields were aggregated to a monthly time scale and empirically fit to a statistical distribution at the grid and monthly scales to define drought. Two indices are computed for drought assessment. The first is the soil moisture based drought index proposed by *Sheffield et al*. [2004]. This drought index, hereby noted as Q_{SM}, is based on the total column soil moisture percentile and has been used as an indicator of agricultural drought in several studies with good results [*Andreadis et al*., 2005; *Sheffield and Wood*, 2007]. Following *Sheffield et al*. [2009], the threshold value taken in this study is the 20th percentile (i.e., an area is in drought if $Q_{SM} < 0.2$). The 20th percentile threshold also is adopted by the U.S. Drought Monitor (Source: National Drought Mitigation Center, University of Nebraska-Lincoln) and has been successfully used in a previous application in the United States [*Andreadis et al*., 2005] and at the continental scale [*Wang et al*., 2011] to identify drought events. Another index widely used for meteorological drought analysis is the standardized precipitation index (SPI). SPI is a measure of standardized departure from the empirical rainfall probability distribution function, which allows one to assess the impact of the individual model's precipitation anomalies across different geographical locations and to make spatial comparisons at different time scales. SPI can be calculated over different time scales allowing for interpretation of drought from monthly to multiyear scales. In our study, 3 month and 12 month SPI (SPI3 and SPI12) are calculated, which represents short-term and long-term precipitation patterns, respectively. *Ntale and Gan* [2003] recommended SPI for eastern Africa based on their comparison of the performance of three drought indicators, including SPI, Palmer Drought Severity Index, and Bhalme-Mooley Index. We define drought at a grid cell if the SPI value is below the threshold of −1.0 [*McKee et al*., 1993].

3.3. Drought Event Identification

A clustering algorithm [*Andreadis et al*., 2005; *Sheffield et al*., 2009] is used to identify drought events that allows for spatially contiguous drought clusters at each time step to merge or divide over time. The clustering algorithm begins with an identification of spatial clusters at each time step, followed by tracking the identified spatial clusters over time. This allows for merging and dividing of clusters during the evolution of a drought (see *Sheffield et al*. [2009] for details). Two threshold values are critical to the identification of the spatial clusters: the drought index threshold (see section 3.2 for details) and a minimum cluster size threshold (hereby noted as N_{grids}). We set the minimum cluster size threshold to be 150 grids ($N_{grids} = 150$ grids; ~1.5% of all grids in our study area), a value adopted previously by *Andreadis et al*. [2006]. Spatial clusters are linked in time based on the extent of overlapping drought areas in neighboring time steps. *Sheffield et al*. [2009] investigated the variability of drought occurrence as defined by the cluster analysis.

3.4. Severity-Area-Duration (SAD) Analysis

Following the identification of drought events during the study period, SAD envelope curves are constructed to profile the extreme drought conditions and describe the maximum severity at different combinations of spatial and temporal resolutions. Severity (S) is defined as follows:

$$S = 1\frac{\sum DI}{t}$$

where DI denotes the drought index (Q_{SM} or SPI, as described in section 3.2) and t (months) as the predefined drought durations, which were set for this analysis at 3, 6, 12, 24, and 48 months. The construction of a SAD curve for a drought event identified by the clustering algorithm starts from the grid cell with the maximum severity. The algorithm then, one-by-one, adds grid cells in the 3×3 neighborhood of any added grids (under drought) starting with the grid with the highest drought severity. After each grid is added, the algorithm records the number of currently included grids and their average severity. This process is repeated until all the grids in the spatial drought cluster are summed. Details of the SAD analysis method can be found in *Andreadis et al*. [2005], *Sheffield et al*. [2009], and *Wang et al*. [2011].

Note that the original SAD algorithm begins with applying a median filter for spatial smoothing. However, applying median filter will smooth out anomalies, decrease the number of drought events, and therefore potentially hide some discrepancies between observation and reanalyses precipitation data sets. For the purpose of this study, the median filter is not employed. As a result, the drought clusters are more spatially scattered.

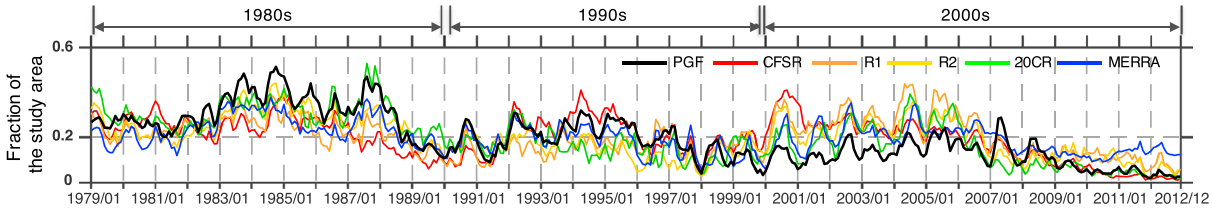

Figure 1. Fraction of sub-Saharan African continent under drought conditions computed from the Q_{SM} data set ($Q_{SM} < 0.2$).

4. Results and Discussion

Figures 1 and 2 provide an overview of drought conditions in sub-Saharan Africa during the period of 1979 to 2012. Figure 1 shows the time series for the fraction of area in drought based on the Q_{SM} derived from VIC soil moisture simulations using different the precipitation forcings from reanalyses. Figure 2 shows the percentage of months under drought during 1980s, 1990s, and 2000s as indicated by Q_{SM}. The three drought episodes were recognized and analyzed in previous studies [*Giannini et al.*, 2008; *Dai*, 2011] and thus are discussed separately in more detail in section 4.1. The false alarm rate (FAR) and probability of detection (POD) in the detection of drought events for African during our study period are shown in Figure 3, benchmarked on the PGF data set. In general, all five reanalyses reproduce major drought events fairly well at the continental scale, with differences in spatial contiguity and temporal persistency, as well as spatial and temporal mismatches in drought occurrence.

There are regional differences in drought detection over sub-Saharan Africa among different data set (Figure 3). Southern Africa droughts are more consistently estimated with high detectability (high POD) and reliability (low FAR). This is most likely due to a larger number of in situ observational stations and upper level radiosondes in the region, with the latter assimilated in the reanalyses. This suggests that the accuracy of reanalyses data is dependent on the observational data availability, that is, reanalyses data is more accurate over well-observed

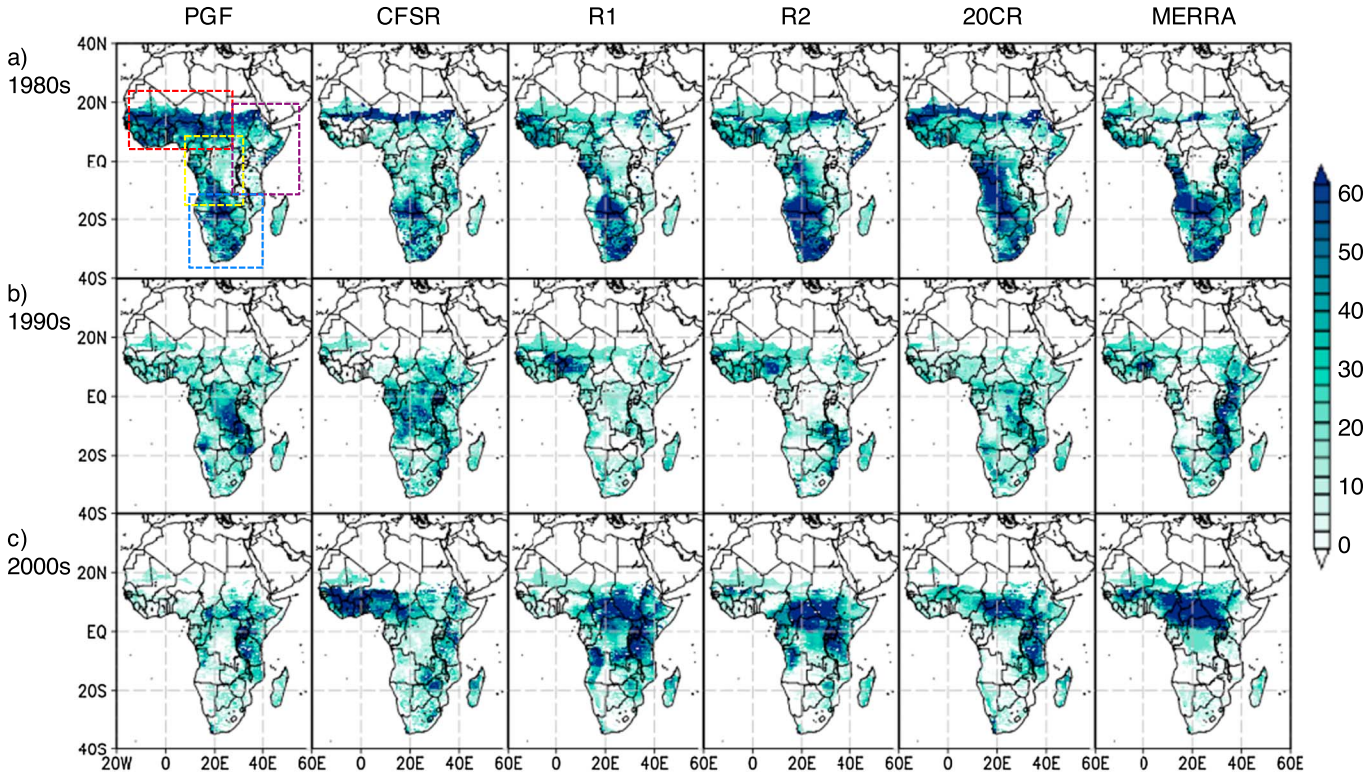

Figure 2. Percentage months in contiguous drought during (a) 1980s, (b) 1990s, and (c) 2000s drought episodes based on PGF and five reanalyses (from left to right, CFSR, R1, R2, 20CR, and MERRA). Line shadings in Figure 2a (left panel) correspond to regions in Table 4.

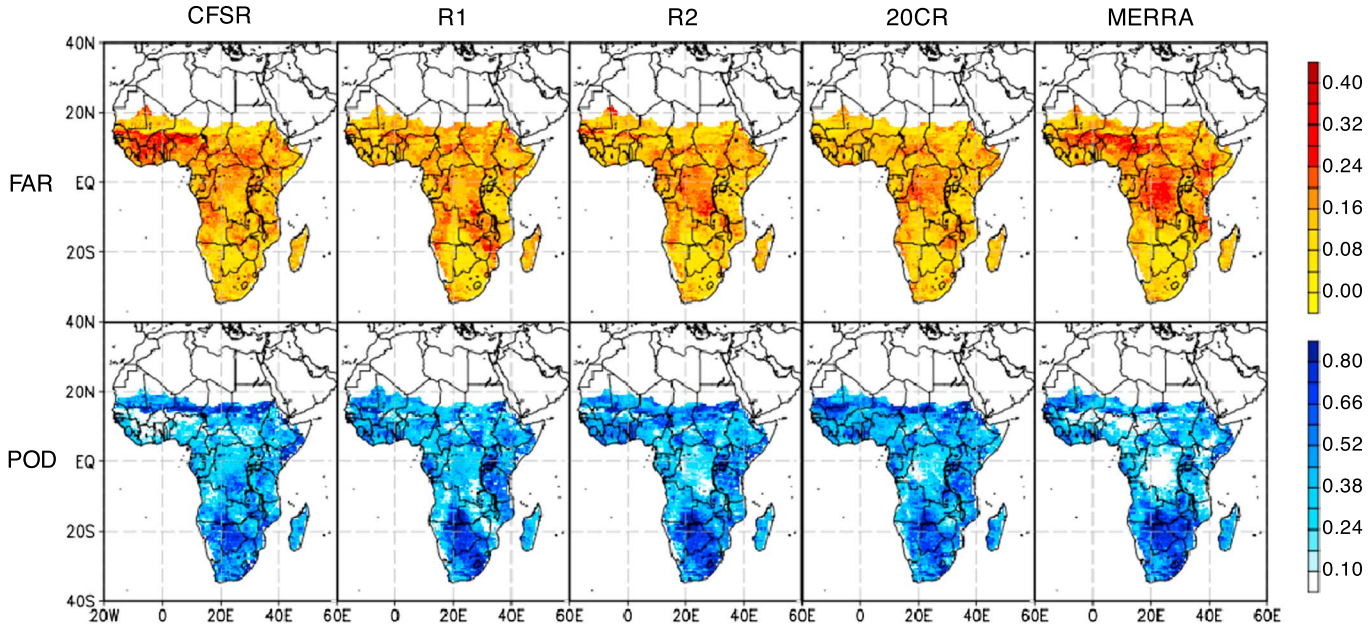

Figure 3. False alarm rate (FAR) and probability of detection (POD) of soil moisture droughts based on Q_{SM} of five reanalyses (CFSR, R1, R2, 20CR, and MERRA) from 1979 to 2012.

regions. On the other hand, despite the relatively few gauge observations, droughts in the Sahel region are also well replicated with high skill (high detectability and reliability). This is likely due to that fact that the drivers of Sahel droughts are better understood based on previous research [*Masih et al*., 2014], and this understanding is reflected in climate models. Mechanisms related to dry conditions in Sahel include El Niño–Southern Oscillation [ENSO; *Nicholson*, 2000, oceans warming in Atlantic and Indian Ocean; *Dai*, 2013], southward shift of Intertropical Convergence Zone (ITCZ) [*Caminade and Terry*, 2010; *Dai*, 2011], land-atmosphere feedbacks, and human activities (aerosol emissions) [e.g., *Desboeufs et al*., 2010]. Timing and spatial extent of eastern African drought events are less satisfactorily reproduced compared to southern Africa, especially by MERRA. Regions with the lowest detectability and reliability in constructed drought events are West and central Africa (Sahel region not included). This coincides with the limited studies on northwestern African drought mechanism [*Masih et al*., 2014]. Further studies on the causes of droughts, both natural drivers and anthropogenic factors, are needed in northwestern Africa (Morocco and northern Algeria).

On the longer-term continental scale, overall statistics of drought events in reanalyses is in reasonably good agreement to that of PGF. Table 2 provides the number of drought events in the reanalyses data sets over the 34 year period. Drought events are partitioned into three categories based on their duration: short-term drought ($<$6 months), medium-term drought (6–11 months), and long-term drought ($\geq$12 months). R1 and 20CR estimate more short-term events and less long-term events, indicating that prolonged drought events tend to break during their evolution. R2 and MERRA, on the other hand, have the fewest short- to medium-term droughts. Since the occurrence of long-term droughts is consistent to PGF, it is inferred that the spatiotemporal coherency of short-to-medium-term droughts in the two reanalyses is more different than the long-term events. Given that the spatial-temporal extent of droughts is the same across different precipitation data sets, this suggests that the droughts depicted by these two reanalyses precipitation data sets extend larger spatially. CFSR does not show significant bias in the occurrence of drought events of different

Table 2. Number of Drought Events Categorized by Duration

	PGF	CFSR	R1	R2	20CR	MERRA
Total	72	74	79	66	77	65
Short-term droughts	54	56	67	51	64	51
Medium-term droughts	10	11	7	7	9	7
Long-term droughts	8	7	5	8	4	7

Table 3. Occurrences of Drought Clusters (Sum of All Time Steps) in PGF, CFSR, R1, R2, 20CR, and MERRA Conditioned on Cluster Sizes

	Small Clusters ($\times 10^4$)	Medium Clusters	Large Clusters
PGF	2.67	310	26
CFSR	3.35	308	16
R1	2.14	319	24
R2	1.96	388	13
20CR	2.18	315	27
MERRA	2.10	373	11

durations. However, it should be noted here that an agreement in the distribution of event duration does not necessarily indicate an accurate depiction of individual drought events nor does this suggest a better representation in the spatial pattern of drought clusters.

The spatial pattern of droughts in CFSR is more scattered than that observed. Since the drought cluster method allows for merging and splitting of clusters during the evolution of an event, the spatial extent of an event at a specific time step may consist of multiple drought clusters that were split from, or will join into, one cluster through the lifetime of the event. We count the occurrence of drought clusters at each time step with respect to cluster sizes. A small cluster is defined as drought clusters with less than 350 contiguous grids; a medium cluster is consisting of 351 to 1750 contiguous grids and a large cluster has more than 1750 contiguous grids. Table 3 shows the number of spatial drought clusters depicted by PGF and the five reanalyses precipitation data sets. CFSR sees more small clusters and less large clusters. The lack of large drought clusters is shared by R1, R2, and MERRA reanalyses data sets. This is due to the low drought severity in the widespread 1980s Sahel droughts (discussed in section 4.1). In addition, R1, R2, 20CR, and MERRA estimate more medium-size clusters but less small clusters, showing discrepancies in the spatial coherency of depicted droughts.

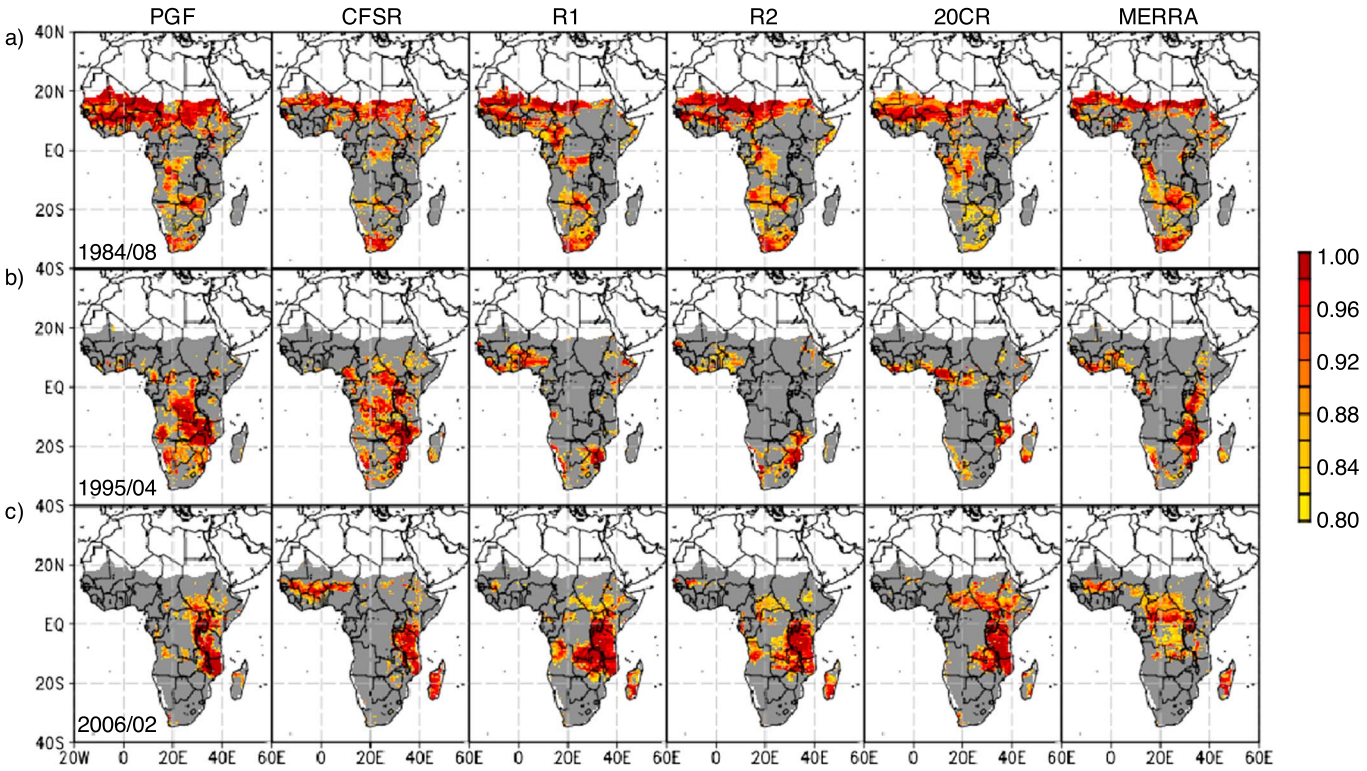

Figure 4. Snapshots of drought conditions in the 1980s, 1990s, and 2000s drought episodes in (a) August 1984, (b) April 1995, and (c) February 2006. The drought condition is depicted by (from left to right) PGF, CFSR, R1, R2, 20CR, and MERRA. Color shading shows drought severity. A higher value corresponds to a higher drought severity.

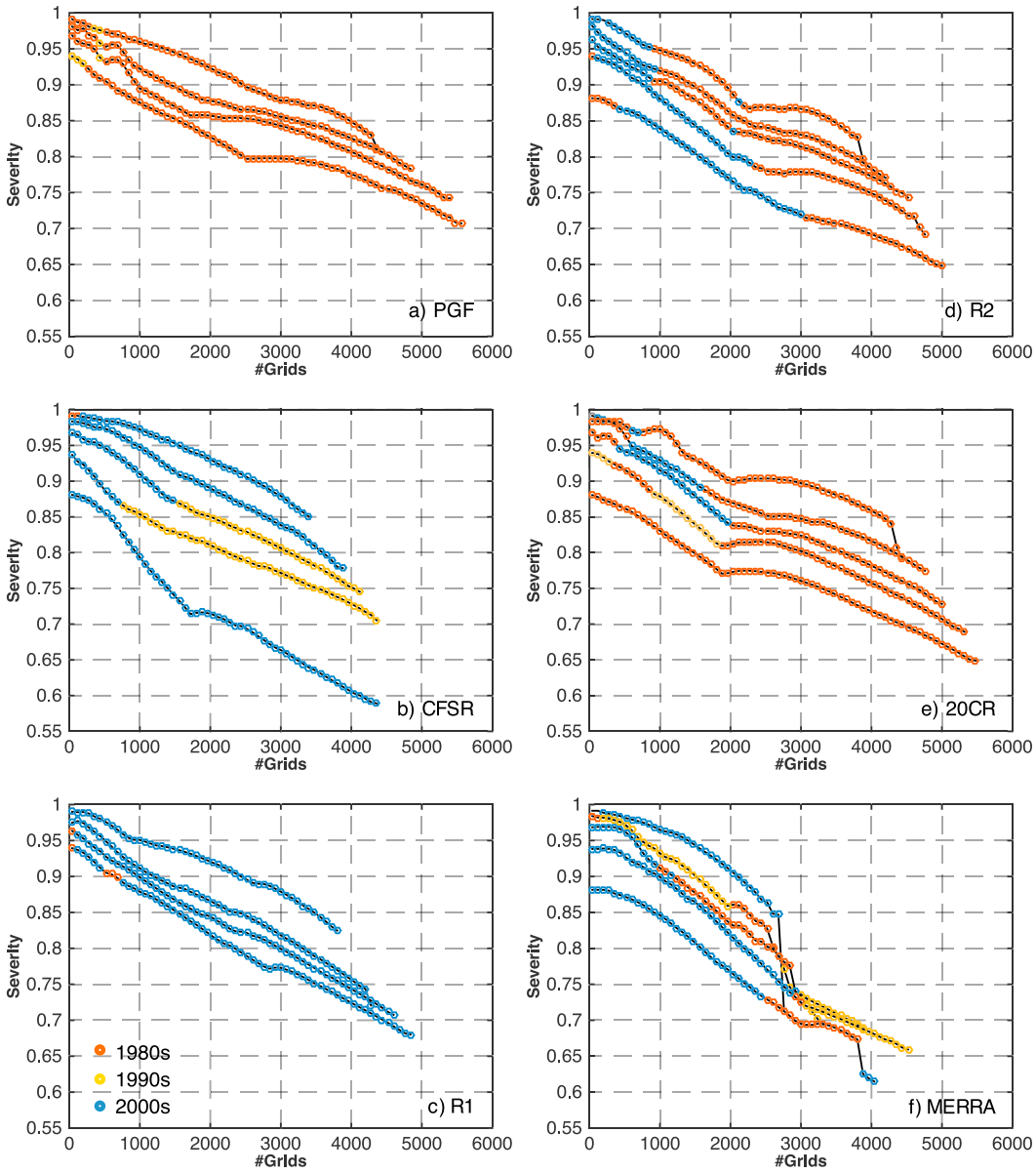

Figure 5. SAD envelop curves of 34 years study period over the sub-Saharan region at (from top to bottom) 3, 6, 12, 24, and 48 month time scale depicted by PGF and five reanalyses precipitation data sets (CFSR, R1, R2, 20CR, and MERRA). Color shading corresponds to different drought episodes.

4.1. Characteristics of Drought Episodes

Our results show that Africa suffered from three severe drought episodes during the 34 years of the study period, each dominated by a spatially extensive drought over different regions. They are the prolonged 1980s Sahel drought, 1990s drought of central Africa, and 2000s eastern Africa drought. A snapshot of each drought episode in PGF and the reanalyses precipitation data sets are provided in Figure 4. The figure shows the areal fraction in drought in reanalyses precipitation data sets at the time when the event in PGF reaches its largest spatial extent. These maps are similar with findings in previous studies that analyzed the geospatial coverage of drought extremes, e.g., *Vicente-Serrano et al.* [2012] using Standardized Precipitation and Evapotranspiration Index. The three major drought episodes and their spatial extents are shown in Figure 1. In PGF, the top three largest and longest drought events come from 1980s, 1990s, and 2000s drought episodes, respectively, which is consistent with the common perception that spatially extensive droughts also tend to last longer and with higher severity. The three severe drought episodes and their relative ranks are consistent with previous studies

[*Rouault and Richard*, 2005; *Kasei et al*., 2010; *Masih et al*., 2014]. Among others, *Masih et al*. [2014] reviewed more than 500 articles and identified the dry conditions in Sahel in 1983–1984 as having the highest severity. According to PGF, the spatial extent of 1980s Sahel megadrought is the largest, affecting approximately 16.64×10^6 km^2 and persisting almost two times longer (91 months, December 1981–August 1988) than the second most severe drought, the 1990s drought (50 months, October 1993–November 1997). The 2000s drought is the least spatially extensive (8.78×10^6 km^2), yet it posed a serious threat to regional food security as a large percentage of agricultural land lay within the affected region. The 2010–2011 drought in Horn of Africa plunged eastern Africa into the worst famine in 20 years and affected more than 11.5 million people [*United Nations Office for the Coordination of Humanitarian Affairs*, 2011]. The relative intensity of 1980s, 1990s, and 2000s drought events is confirmed by the SAD envelope curves shown in Figure 5, which provides a regional severe drought profile as constructed by combining different drought events at different areal extents via the SAD methodology. The 1980s drought is the most intense event as it dominates the SAD envelope curves for its large extent and at all durations; while the 1990s drought contributed to a small number of points in SAD envelope curve at very small spatial areas.

The spatial pattern of drought events in CFSR is more scattered than that observed. The results indicate that the contiguous drought area of 1990s drought does not span as large an area as the 1980s. However, instead of a further decrease in the affected area, the spatial extent of the 2000s drought is significantly larger from the reanalyses (Figure 1). In general, reanalyses estimate a wetter 1980s, a significantly drier 2000s, and comparable conditions in the 1990s compared to PGF. Thus, the 2000s drought in reanalyses is significantly more intensive in both duration and spatial extent than the 1980s Sahel megadrought. Severity of the 2000s drought in reanalyses is higher than the 1980s as well. As is shown in Figure 5, the 2000s drought dominates most of the SAD envelope curves for CFSR, R1, and MERRA, while R2 and 20CR replicate its intensity but with a longer duration and smaller the spatial extent. Similarly, for the 1990s drought as its severity is ranked lower, with the exception of CFSR and MERRA.

On the other hand, discrepancies exist in the spatial pattern of drought events depicted by reanalyses in comparison to observations (i.e., PGF-based estimates.) Figure 6 shows the same SAD envelope curves as Figure 5 but color shaded by the location of grids that are experiencing drought. There are large differences in the location of the drought events at different spatial extents and time scales. In PGF (Figure 6a), at 6 month and longer time scales, the SAD envelope curves at the large spatial extent is composed from the southern African drought, while the 1980s Sahel drought dominants the rest of the curves at smaller spatial scales. However, although 20CR agrees with PGF that the 1980s drought is the most severe event, the location of the severe drought is different from that in PGF. The majority of the 20CR SAD envelope curves (Figure 6e) at large spatial scales are composed by drought over the central Africa region. With a closer look, discrepancies can be found in the reproduced drought events by reanalyses data sets in each dry period.

4.1.1. The 1980s Sahel and Southern Africa Drought

As the most significant disaster during the study period, the 1980s Sahel drought has led to widespread famine affecting millions of people [*Sheffield et al*., 2006; *Kasei et al*., 2010; *Masih et al*., 2014]. The reanalyses precipitation data sets perform fairly well in terms of locating the drought over both the Sahel and southern Africa (Figure 2a). In PGF, we find that the 1980s drought (snapshot shown in Figure 4a) began in December 1980 in two nonadjacent regions: southern Africa and the Sahel. The southern Africa drought then evolved and migrated northward until it joined with Sahel drought in 1982, soon after which the droughts split and evolve separately in 1983. The Sahel drought reached its maximum spatial extent in 1983–1984 and dissipated in December 1988. Southern Africa drought peaked in 1985–1986 and persisted until the end of 1989.

However, the evolution of the 1980s droughts and the merging and spitting of the southern African and Sahel drought is less well depicted by the CFSR-based estimate. CFSR depicts the Sahel and southern Africa droughts as two separate events that never meet each other spatially during their existence. This results in a significantly smaller estimation of the maximum spatial extent of this drought event (12.64×10^6 km^2) in CFSR. Another feature of the 1980s drought in CFSR is the persistence of a high-severity drought center. The drought center, located over the border of Angola and Zambia, decreases little in severity over the event and persisted for almost 3 years until it suddenly disappeared. The evolution of this drought is fairly well replicated by R1, R2, 20CR, and MERRA, with differences being in the timing and spatial pattern of their drought severity. In R1, the southern Africa branch lasts longer than PGF as it started 1 year earlier (January 1980); while the Sahel branch has a shorter duration and dissipated seven months earlier (January 1988)

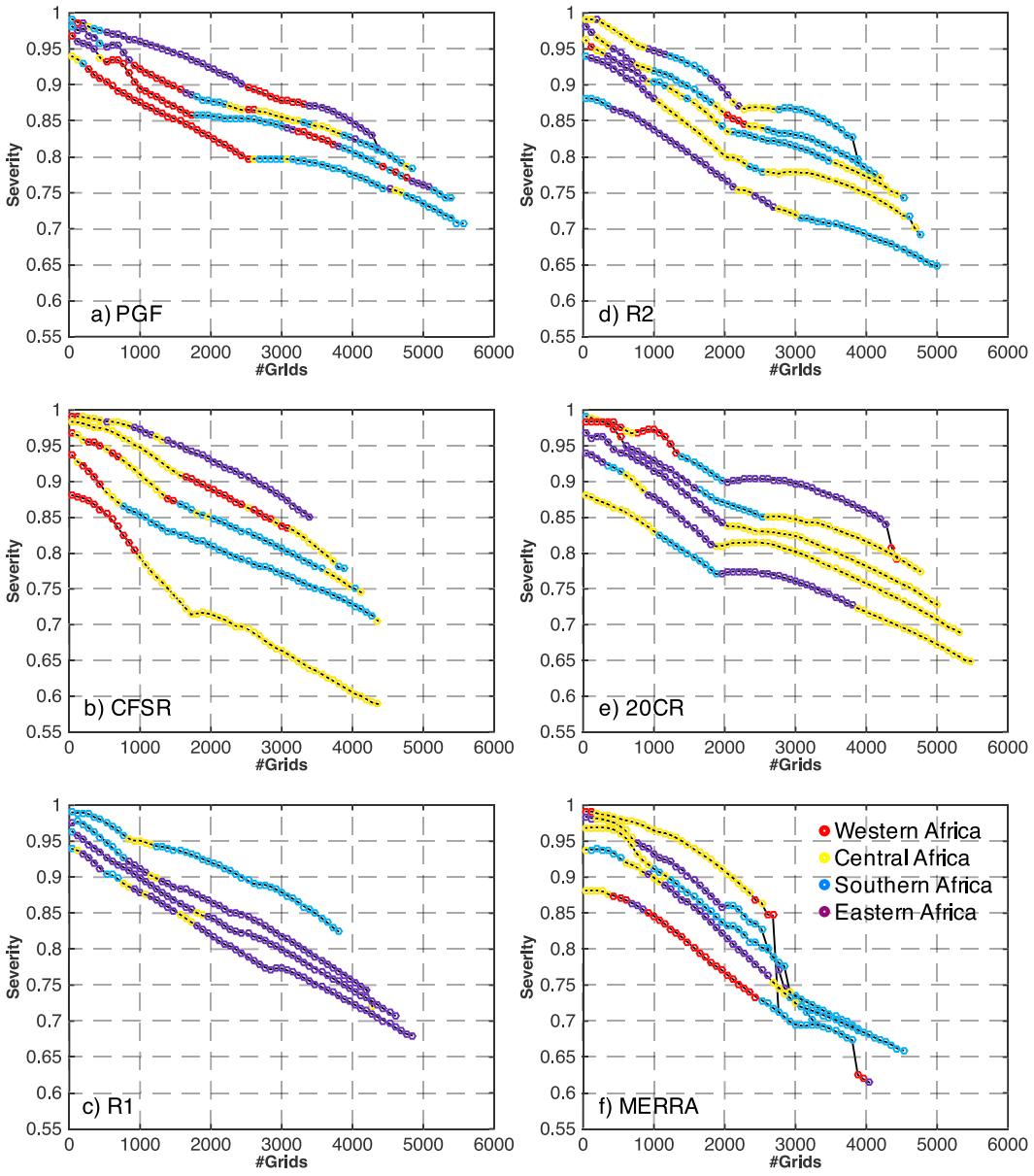

Figure 6. Same as Figure 5, with color shadings representing different geographic locations. The extent of regions is shown in Figure 2a (left panel).

than in PGF. Therefore, the 1980s SAD envelope curves at 24 month and longer time scales (not shown) are taken up entirely by the southern Africa branch. Another noticeable feature in the R1 SAD envelope curves is that they appear "bumpier," unlike the "smoothness" in the PGF-based SAD curves. Upon closer inspection, it is because the R1 curves are derived from droughts at different times and locations during the drought existence. This implies that superimposed on the interannual drought dynamics, R1 shows continuous, high-frequency fluctuations in drought severity. The fluctuations appear temporally for southern Africa and both spatially and temporally over the Sahel. R2 performs similarly to R1 but with a lower wet bias. However, on the relative severity between southern Africa drought and the Sahel drought, the latter is almost always lower, and it barely appears in the SAD envelope curves. This is most likely because the northward latitudinal shift of the West Africa rain belt moves beyond the study area in our analysis. The southern Africa drought recovered slowly after 1988 and evolved into a persistent drought into the 1990s resulting in a much longer lasting drought event that lasted until May 1993. Of all the five reanalyses data sets, 20CR reproduces the 1980s drought closest to PGF in terms of its estimated severity and spatial extent.

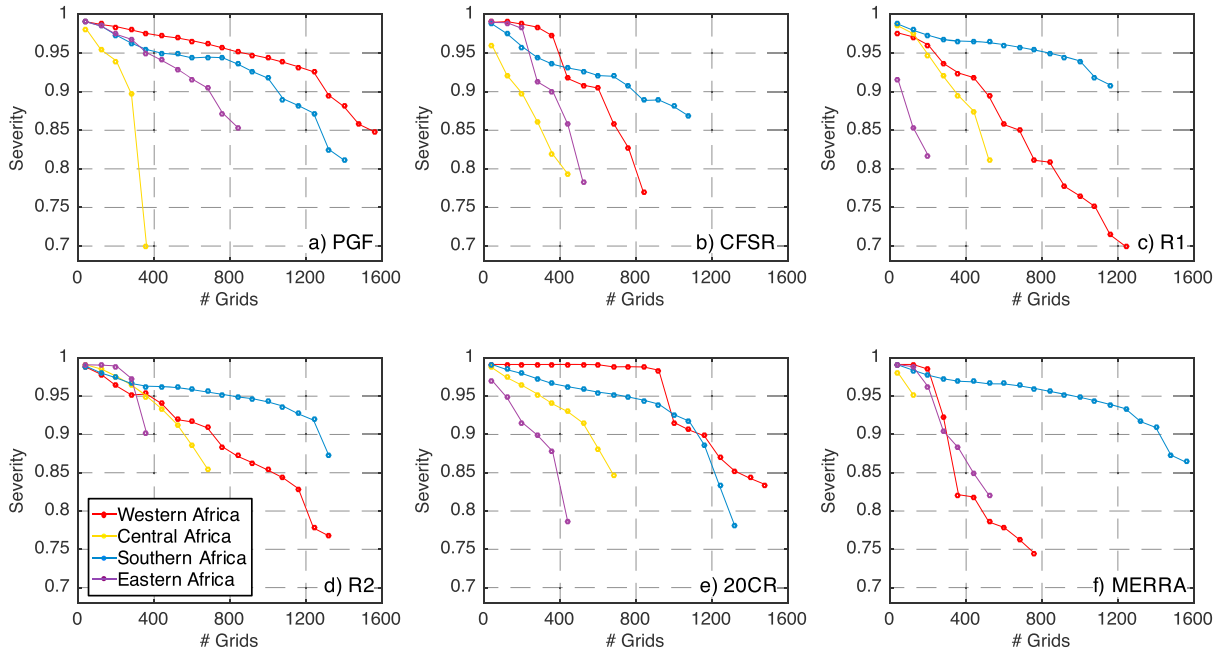

Figure 7. The 6 month SAD envelope curves of the 1980s drought period over the western, central, southern and eastern Africa region depicted by (a) PGF, (b) CFSR, (c) R1, (d) R2, (e) 20CR, and (f) MERRA precipitation data sets. Line colors correspond to geographic locations shown in Figure 2a (left panel).

Differences in its depiction mainly occur after 1986. During 1986 to 1989, instead of further recovering from the earlier drought peak, the southern Africa drought in 20CR came back in late 1987 but with a lower severity than the 1983–1984 peak. This return gives rise to the persistence of this event, lasting much longer—until May 1991. MERRA has the least severe drought (i.e., a wet bias) among the five reanalyses throughout the 1980s. The background wet bias results in the significantly smaller estimation of the maximum spatial extent. On the other hand, there are more drought events/clusters with smaller average sizes in MERRA, which suggest that MERRA does not represent well the spatial rainfall patterns, at least over this period.

After the cluster analysis, we separate the study area into four regions, (western, eastern, central, and southern Africa, as shown in Figure 2) and then construct SAD envelope curves for each region. Figure 7 shows the 6 month SAD envelope curves of 1980s drought over four regions in Africa: western, eastern, southern, and central Africa. It is clear that the severity of Western Africa drought, namely, the Sahel drought, is the highest among the four regions, followed by the southern Africa region (Figure 7a). Relatively smaller area in eastern and central Africa region suffers from dry condition with relatively lower severity. Except for the 20CR, the Sahel drought is significantly less spatially extensive in reanalyses with a lower severity that results in a corresponding lower long-term drought risk. Meanwhile, reanalyses, especially R1 (Figure 7c), R2 (Figure 7d), and MERRA (Figure 7f) estimate more intense, dry conditions in southern African. R1 and R2 depict the southern Africa drought with a higher severity than the Sahel drought at all spatial extents. CFSR (Figure 7b), 20CR (Figure 7e), and MERRA (Figure 7f) estimate higher severity in the center of the Sahel drought than they do in southern Africa, but the severity gradient degrades faster as the drought area expands and with the severity becoming lower than the southern Africa branch at larger spatial extents. In particular, the high-severity drought center in MERRA is not spatially extensive with the SAD envelope curves showing a steep decrease in severity (slope) with increased area under drought.

4.1.2. The 1990s Central Africa Drought

The 1990s drought is the second most severe event depicted by the PGF-based analysis affecting mainly central Africa (Figure 2b). The event began, intensified, peaked, and dissipated with little spatial migration, and it reached its maximum spatial extent in April 1995 (a snapshot provided in Figure 4b). In PGF, the region ended the drought in July–September of 1997, but the dry spell persists much longer in R1 and 20CR (until 1999). Their 1990s SAD curves (not shown) is made up by droughts located in western Africa, as opposed to PGF curves which are primarily derived from the central Africa region. Therefore, the SAD curves from the reanalyses data sets are radically different in shape when compared to PGF. This suggests that the interannual

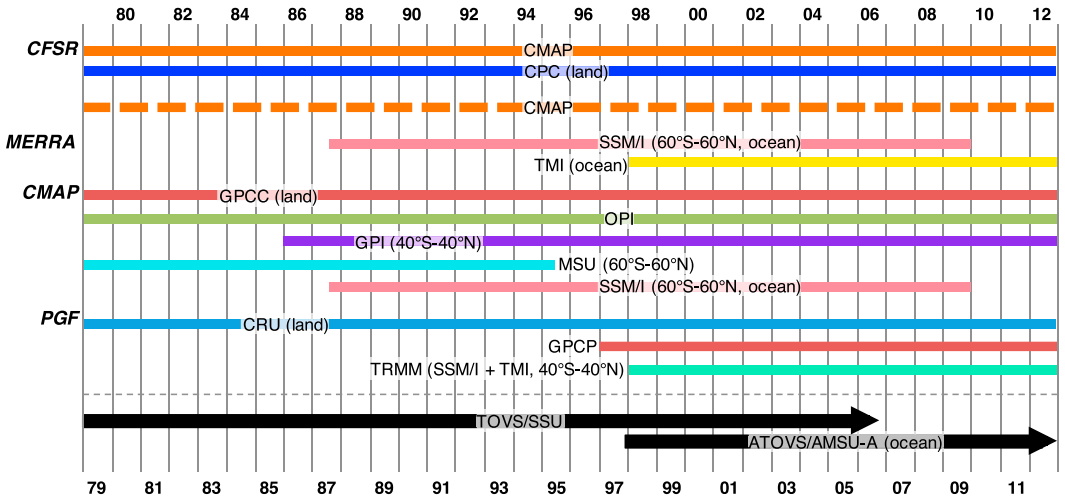

Figure 8. Temporal and spatial coverage of observational precipitation data sets included in reanalyses assimilation systems (namely, CFSR, R2, and MERRA) and contributing data sets in the development of two observation-based data sets (CMAP and PGF). Dashed line indicates that the precipitation observation is used to adjust the initial land conditions instead of directly assimilated to correct precipitation. Black arrows represent the change in assimilated radiance data from TOVS/stratospheric sounding unit before 2006 to include ATOVS/advanced microwave sounding unit-A radiance data after 1998.

variability and persistence in the central and West Africa rain belt is significantly different in the two reanalyses, especially R1, compared to PGF. CFSR and 20CR, though to a lesser extent, also estimate less drought occurrence in 1990s central Africa region.

4.1.3. The 2000s Eastern Africa Drought

The 2000s drought over the Horn of Africa and part of central Africa was the least extensive, both spatially and temporally, among the three episodes being analyzed (Figure 1). However, depiction of the 2000s drought by reanalyses features a significant dry bias as compared to PGF. Two droughts stand out, which occurred in 2000 and 2005, respectively. The latter is relatively more intense (spatially extensive and temporally persistent). The year 2000 was in the cold phase of ENSO, resulting in a dry eastern Africa [*Dutra et al*., 2013; *Tierney et al*., 2013]. The region suffered from another severe drought during its 2005 "short rains" (October to November.) There is agreement among reanalyses data sets that equatorial East Africa has the most frequent drought occurrence after 2000, but with differences in drought intensity.

4.2. Availability and Changes in the Reanalyses Assimilation Systems

It is likely that differences in drought depiction, especially the 1990s drought episode, are related to the observational data included in reanalyses systems, in particular, precipitation observations. Reanalyses precipitation is the primary forcing for the off-line land surface analysis rather than a state variable. Figure 8 provides a list of precipitation observations included by different reanalyses systems as well as the component data sets of CMAP [*Xie and Arkin*, 1997] and PGF [*Sheffield et al*., 2006] precipitation. In the R1 and 20CR, precipitation products are rainfall forecasts from coupled atmospheric and oceanic models with no direct assimilation of precipitation observations. SAD curves of the 1990s drought from the two reanalyses products are more different than the other reanalyses when using PGF as the reference. In R2, CFSR, and MERRA, a number of different precipitation observations from conventional gauge observations, in situ, and satellite observations are included. R2 takes rainfall observation from 5 day CMAP precipitation to adjust initial land conditions. CFSR and MERRA, unlike R2, directly assimilate precipitation observations to correct the precipitation forecast. CFSR blends model forecast with the same 5 day CMAP precipitation [*Xie and Arkin*, 1997] used by R2 and the daily CPC unified global gauge analysis [*Xie et al*., 2007; *Chen et al*., 2008] to drive GLDAS/LIS. The former is especially favored in the tropics, while the latter is given higher weight in high latitudes. The blended precipitation product is used to force Noah LSM within NCEP's GLDAS/LIS system. MERRA utilized newly available satellite precipitation estimates from the TMI and SSM/I for a tendency correction over the oceans within the incremental analysis update framework

Table 4. Average Number of Observation Stations Available in Different Regions and Skills Indicated by False Alarm Rate (FAR) and Probability of Detection (POD) in Reanalyses Precipitation Using PGF as Reference[a]

		CFSR		R2	
	GPCC Stations	FAR	POD	FAR	POD
Central Africa	60	0.16	0.37	0.17	0.30
Eastern Africa	369	0.14	0.42	0.13	0.47
Western Africa	582	0.17	0.32	0.14	0.44
Southern Africa	1093	0.13	0.49	0.12	0.53

[a]GPCC provides the number of rain gauge stations per grid with its gridded gauge-analysis precipitation product [*Xie et al.*, 2007; *Chen et al.*, 2008]. The spatial extent of different regions is shown in Figure 2a (left panel).

The central African region has the lowest POD and highest FAR compared to other regions in sub-Saharan Africa (Figure 3). The prevailing drought condition in central Africa captured by PGF is almost completely missed by R1, R2, and MERRA. CFSR and 20CR, though to a lesser extent, also have less drought occurrence in 1990s for this region (Figure 2b). Aside from the limited knowledge of drivers of central African drought, the regional difference in the skill of drought depiction (i.e., lower skill in central Africa) is related to the availability and consistency of precipitation measurements included in the assimilation systems. As discussed earlier, CFSR and R2 take advantage of CMAP precipitation estimates. CMAP is obtained by merging Global Precipitation Climatology Center (GPCC) gauge stations [*Xie and Arkin*, 1995], five satellite estimates from the GOES Precipitation Index (GPI) [*Arkin and Meisner*, 1987], outgoing longwave radiation-based precipitation index [*Xie and Arkin*, 1997], SSM/I [*Grody*, 1991; *Ferraro et al.*, 1994; *Wilheit et al.*, 1991] and microwave sounding unit (MSU) [*Spencer*, 1993], and R1 reanalysis precipitation from numerical forecast models. Table 4 shows the relationship of GPCC gauge observation availability (number of GPCC gauge stations in CMAP) and bias in regional precipitation. Drought events in central Africa, where the least amount of observations are available compared to other regions, are more diversely depicted by CFSR and R2 versus PGF. This indicates that the observational data availability plays an important role in the development of accurate long-term reanalyses data products. It appears that the abrupt change in precipitation and temperature after 1999 is closely related to the inclusion of the new Advanced TIROS Operational Vertical Sounder (ATOVS) observation data in the reanalyses assimilation systems. *Zhang et al.* [2012] demonstrated that the sudden increase in precipitation over the oceans, as well as increase in precipitable water and low-level specific humidity around 1998, is due to the inclusion of ATOVS radiance data in the assimilation systems for CFSR, R2, and MERRA. Changes in precipitation afterward are the results of the interplay between a lack of calibration of the forecast and the assimilation system with the new sensor data. Notably, CFSR after 1999 has dramatically enhanced interannual variability in precipitation suggesting an intensified water cycle, while R2 is less affected (Figure 9). It is likely due to the soil moisture nudging scheme of R2 that lowers the impact of abrupt changes in the observation data. Furthermore, on top of the impact induced by the inclusion of ATOVS radiance data, MERRA also started to ingest satellite rain rate estimates from TMI and SSM/I over the oceans in 1998 (Figure 9). Thus, changes in rainfall amounts and variability, particularly in the period of 2000 to 2007 (Figure 9), are likely a result of changes in the assimilated data.

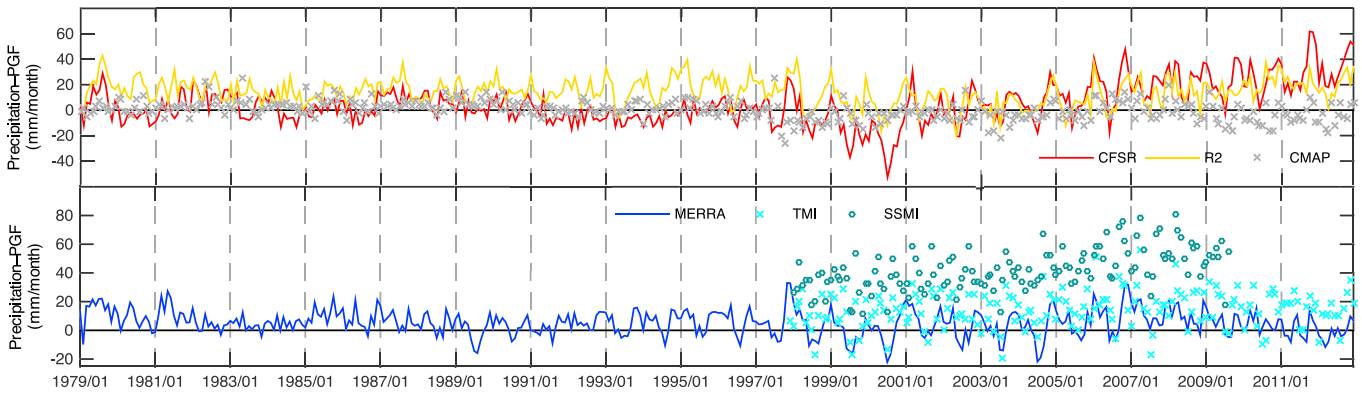

Figure 9. Time series of domain average precipitation difference between PGF and CFSR and MERRA with their associated precipitation observations.

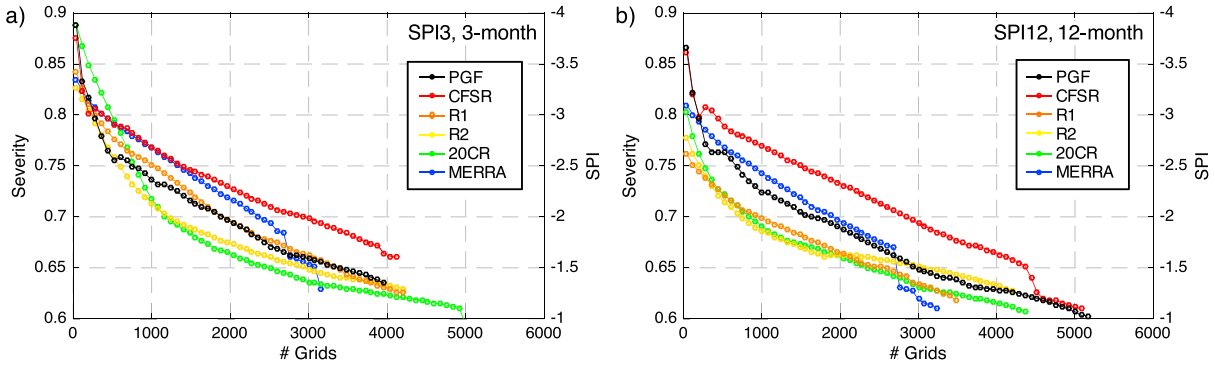

Figure 10. SAD envelope curves based on (a) SPI3 at 3 month time scale and (b) SPI12 at 12 month time scale.

4.3. Drought Depiction Based on SPI

More insights on the role of precipitation forcing for soil moisture anomalies can be given by a SAD analysis based on SPI.

There are discrepancies shown in the spatial patterns of SPI at different time scales and among different reanalyses data. Figure 10a shows SAD envelope curves at a 3 month time scale based on SPI3 and at 12 month time scale based on SPI12. For example, the 3 month SAD envelope curve (Figure 10a) is derived from drought clusters with the 3 month-averaged SPI3 values falling below the threshold of −1. Figures 10a and 10b represent the maximum precipitation anomaly of short-term and long-term drought, respectively. Results show discrepancies in the spatial pattern of SPI. Short-term dry extremes defined by SPI3 are more severe in reanalyses than in PGF. Compared to PGF, R2, and 20CR estimate larger maximum spatial extent, while CFSR, R1, and MERRA estimate higher drought severity. This strong evidence that the anomalies of reanalyses precipitation data sets have higher spatial correlation due to higher monthly-to-seasonal rainfall variability (Figure 9). However, the more intense drought condition is not present at the 12 month time scale (Figure 10b). That is, except for CFSR, extremes in 12 month-average SPI12 depicted by reanalyses products is lower than PGF with smaller maximum spatial extent, as the stronger short-term anomalies average out. For CFSR, rainfall variability is higher at both short-term and long-term time scale.

In summary, the discrepancies in SPI-defined droughts originated from differences in precipitation variability and spatial correlation of precipitation anomalies, in reanalyses data sets. The monthly-to-seasonal rainfall variability is enhanced in reanalyses. However, when aggregated in time (≥12 month), the anomalies are averaged out, and the dry extremes at 12 month or longer time scales are less severe in all reanalyses, except for CFSR, than in PGF. CFSR, on the other hand, depicts a more severe dry extreme at both short-term and long-term time scale.

4.4. Uncertainties in Drought Identification and SAD Analysis

4.4.1. Drought Identification Parameterization

The choice of different thresholds used in defining droughts can cause uncertainties in the results. Currently, we have two threshold parameters that are used in our study. The first parameter is the threshold on drought index values used to distinguish severe drought events [*Sheffield et al*., 2009]. The value adopted for Q_{SM} corresponds to the commonly used 20th percentile and for SPI the value of −1. These values have been extensively and successfully used to capture and describe drought events in a number of studies [e.g., *Sheffield and Wood*, 2008; *Lloyd-Hughes and Saunders*, 2002].

Another threshold used in the spatial-temporal identification of drought events is the minimum contiguous area affected by drought. *Vidal et al*. [2009] recommends a threshold of percent area of the study area. The value adopted for Africa is 150 half-degree grid cells (approximately 375,000 km^2, ~1.5% of Africa). Previous studies have picked a minimum cluster area threshold of 500,000 km^2 (approximately fifty 1° grids or 2% of Africa) [*Sheffield et al*., 2009]. *Sheffield et al*. [2009] found large reduction in the number of events when increasing the cluster area threshold from 100,000 km^2 to 500,000 km^2, suggesting a large percentage of drought events have a maximum spatial extent within this range. Due to differences in settings, it is difficult to directly compare the outcome of drought depiction to results in [*Sheffield et al*., 2009]. However, the

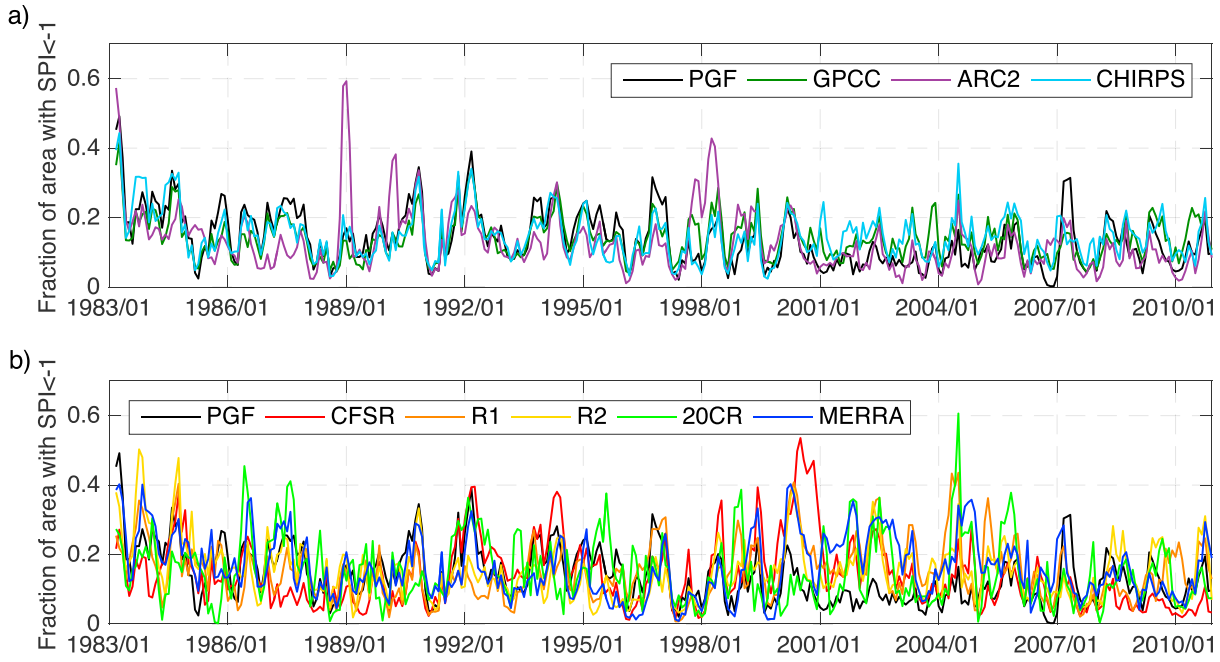

Figure 11. Fraction of sub-Saharan Africa area under drought (SPI < -1) based on PGF and (a) observational data sets from GPCC, ARC2, and CHIRPS; (b) reanalyses precipitation data sets from CFSR, R1, R2, 20CR, and MERRA.

longest duration and peak extent in this study is reasonably reproduced compared to that in *Sheffield et al.* [2009] with slight overestimation due to a finer resolution in the LSM simulations.

4.4.2. Uncertainties in PGF

PGF data show that 2000s is in a relatively wetter period compared to previous periods in the study (1980s or 1990s); however, none of the reanalyses show the wetting trend as strongly as PGF. To examine the reliability of PGF precipitation data, we compared SPI3 based on PGF to that derived from the gridded observational precipitation data from the GPCC gridded monthly precipitation data set [*Xie and Arkin*, 1997], Africa Rainfall Climatology version 2 (ARC2) [*Novella and Thiaw*, 2013], and Climate Hazards Group Infrared Precipitation with Station data (CHIRPS) [*Funk et al.*, 2015]. Figure 11 shows the fraction of drought area defined as a SPI3 value smaller than -1. The four time series from PGF, GPCC, ARC2, and CHIRPS (Figure 11a) are close to each other, compared to the reanalyses data sets in Figure 11b. The result confirms the relatively wetter condition after 2000 as a smaller dry area is observed by all four observational rainfall data set. Ideally, the reference precipitation data would be taken from a sufficiently densely gauged, observation-based source that is independent to the five reanalyses data sets in consideration. However, given the limited in situ data availability and the reanalyses observation systems, it is infeasible to use a reference data set that is strictly independent of all reanalyses. Given this, PGF is arguably the best estimate currently available with long-term records and global coverage. In the meantime, we acknowledged the existence of unknown bias and errors in the reference data set especially over the data sparse regions of Africa in the most recent past.

5. Conclusions

Reanalyses' precipitation is routinely used as a surrogate for observations due to its high spatial and temporal resolution, continuous record, and global coverage and thus is widely used in hydrologic and agricultural applications. Yet the resultant products and their reliability are largely dependent on the consistency of reanalyses precipitation data sets. In this study, we addressed the uncertainties in drought identification by reanalyses rainfall products over sub-Saharan Africa and the associated impact on the estimation of drought conditions as measured by the extent, severity, and duration of individual drought events. We evaluated the depiction of drought using five reanalyses precipitation data sets (CFSR, NCEP/NCAR R1, NCAR/DoE R2, 20CR, and MERRA) against drought estimated from the Princeton Global Forcing (PGF) data set, in which the

precipitation data are from combined satellite-gauge based measurements. The precipitation data sets were used to force the Variable Infiltration Capacity (VIC) land surface model to develop fields of soil moisture at a daily and 0.5° spatial resolution that were then used to analyze soil moisture-based drought across Africa from 1979 to 2012. Following the approaches of *Andreadis et al*. [2006], the severity-area-duration (SAD) envelope curves representing the largest events form the basis for the SAD analysis and are used to describe the spatial-temporal characteristics of the identified events at different spatial and temporal scales. The procedure is later repeated using standardized precipitation index (SPI) as the drought index to quantify the role of precipitation in soil-moisture drought depiction.

In general, the statistics of drought spatial-temporal characteristics over the 34 year study period is well reproduced by all five reanalyses data sets. Major drought episodes with severe and prolonged soil moisture droughts are accurately located in time and space by reanalyses, including the 1980s megadrought affecting the Sahel and southern Africa, the 1990s central Africa drought, and the 2000s eastern Africa drought. However, discrepancies are found in the representation of the spatial-temporal characteristics of drought events in dry episodes across the reanalyses products. Regional differences in drought depiction skill are found, with all five reanalyses products having more discrepancies in the depiction of the 1990s central Africa drought. CFSR shows the least differences when compared to PGF, while R1 estimated little dry conditions over the Great Rift Valley in the 1990s. It is likely that this is related to the availability of observational data included in the assimilation system. Central Africa, where limited in situ precipitation observations are available, has large discrepancies compared to the PGF reference data. By evaluating the depiction of meteorological drought based on SPI, discrepancies are attributed to higher monthly to seasonal rainfall variability and differences in spatial correlation of drought conditions from the reanalyses precipitation. The monthly precipitation variability is enhanced in all five reanalyses, while the spatial correlation of drought conditions at short-term time scales is higher. At the 12 month time scale, the correlation is lower except for CFSR, which estimates a higher spatial correlation at both short-term and long-term time scales. The high monthly precipitation variability further increases after about 1999 causing the 1980s drought to have relatively lower intensity and the 2000s drought episode to stand out in both severity, maximum spatial extent, and duration. This is most likely due to changes in input observations used in the reanalyses assimilation systems at around 1999.

The analysis examined the impact of uncertainties in reanalyses precipitation on drought monitoring. The consistency of reanalyses precipitation data is limited by observational data availability and uncertainties associated with the assimilation methods. Caution is needed when using reanalyses precipitation for drought analysis, especially for case studies focusing on specific events at monthly to seasonal time scale. In summary, the results suggest the need for improved bias correction schemes for errors in both the mean (systematic) and variability from the reanalyses products, as well as concerns with the temporal evolution of observation systems used in data assimilation systems. Further studies are needed to better understand and attribute the differences in drought depiction by reanalyses data sets.

Acknowledgments

This research was supported through NASA grant NNX13AG97G (Multi-Sensor Enhancement of Real-Time Satellite Precipitation Retrievals for Improved Drought Monitoring) and NOAA grant NA14OAR4310219 (Development of a Global Flood and Drought Catalogue for the 20th and 21st Centuries). Data used in this paper are available upon request from the authors.

References

Adler, R. F., C. Kidd, G. Petty, M. M. Morrissey, and M. H. Goodman (2001), Intercomparison of global precipitation products: The Third Precipitation Intercomparison Project (PIP–3), *Bull. Am. Meteorol. Soc.*, *82*(7), 1377–1396, doi:10.1175/1520-0477(2001)082<1377:IOGPPT>2.3.CO;2.

Andreadis, K. M., E. A. Clark, A. W. Wood, A. F. Hamlet, and D. P. Lettenmaier (2005), Twentieth-century drought in the conterminous United States, *J. Hydrometeorol.*, *6*(6), 985–1001, doi:10.1175/JHM450.1.

Andreadis, K. M., E. A. Clark, A. W. Wood, A. F. Hamlet, and D. P. Lettenmaier (2006), Twentieth-century drought in the conterminous United States, *J. Hydrometeorol.*, *6*(6), 985–1001, doi:10.1175/JHM450.1.

Arkin, P. A., and B. N. Meisner (1987), The relationship between large-scale convective rainfall and cold cloud over the Western Hemisphere during 1982–84, *Mon. Weather Rev.*, *115*(1), 51–74, doi:10.1175/1520-0493(1987)115<0051:TRBLSC>2.0.CO;2.

Betts, A. K., M. Zhao, P. A. Dirmeyer, and A. C. M. Beljaars (2006), Comparison of ERA40 and NCEP/DOE near-surface data sets with other ISLSCP-II data sets, *J. Geophys. Res.*, *111*, D22S04, doi:10.1029/2006JD007174.

Betts, A. K., M. Köhler, and Y. Zhang (2009), Comparison of river basin hydrometeorology in ERA-Interim and ERA-40 reanalyses with observations, *J. Geophys. Res.*, *114*, D02101, doi:10.1029/2008JD010761.

Bosilovich, M. G., J. Chen, F. R. Robertson, and R. F. Adler (2008), Evaluation of global precipitation in reanalyses, *J. Appl. Meteorol. Climatol.*, *47*(9), 2279–2299, doi:10.1175/2008JAMC1921.1.

Caminade, C., and L. Terray (2010), Twentieth century Sahel rainfall variability as simulated by the ARPEGE AGCM, and future changes, *Clim. Dyn.*, *35*(1), 75–94, doi:10.1007/s00382-009-0545-4.

Chaney, N. W., J. Sheffield, G. Villarini, and E. F. Wood (2014), Development of a high-resolution gridded daily meteorological dataset over sub-Saharan Africa: Spatial analysis of trends in climate extremes, *J. Clim.*, *27*(15), 5815–5835, doi:10.1175/JCLI-D-13-00423.1.

Chen, M., W. Shi, P. Xie, V. Silva, V. E. Kousky, R. Wayne Higgins, and J. E. Janowiak (2008), Assessing objective techniques for gauge-based analyses of global daily precipitation, *J. Geophys. Res.*, *113*, D04110, doi:10.1029/2007JD009132.

Compo, G. P., et al. (2011), The twentieth century reanalysis project, *Q. J. R. Meteorol. Soc.*, *137*(654), 1–28, doi:10.1002/qj.776.
Dai, A. (2011), Drought under global warming: A review, Wiley Interdiscip, *Rev. Clim. Change*, *2*(1), 45–65, doi:10.1002/wcc.81.
Dai, A. (2013), Increasing drought under global warming in observations and models, *Nat. Clim. Change*, *3*(1), 52–58.
Desboeufs, K., E. Journet, J. L. Rajot, S. Chevaillier, S. Triquet, P. Formenti, and A. Zakou (2010), Chemistry of rain events in West Africa: Evidence of dust and biogenic influence in convective systems, *Atmos. Chem. Phys.*, *10*(19), 9283–9293, doi:10.5194/acp-10-9283-2010.
Dutra, E., P. Viterbo, and P. M. A. Miranda (2008), ERA-40 reanalysis hydrological applications in the characterization of regional drought, *Geophys. Res. Lett.*, *35*, L19402, doi:10.1029/2008GL035381.
Dutra, E., L. Magnusson, F. Wetterhall, H. L. Cloke, G. Balsamo, S. Boussetta, and F. Pappenberger (2013), The 2010–2011 drought in the Horn of Africa in ECMWF reanalysis and seasonal forecast products, *Int. J. Climatol.*, *33*(7), 1720–1729, doi:10.1002/joc.3545.
Ek, M. B., K. E. Mitchell, Y. Lin, E. Rogers, P. Grunmann, V. Koren, G. Gayno and J. D. Tarpley (2003), Implementation of Noah land surface model advances in the National Centers for Environmental Prediction operational mesoscale Eta model, *J. Geophys. Res.*, *108*(D22), doi:10.1029/2002JD003296.
Fekete, B. M., C. J. Vörösmarty, J. O. Roads, and C. J. Willmott (2004), Uncertainties in precipitation and their impacts on runoff estimates, *J. Clim.*, *17*(2), 294–304, doi:10.1175/1520-0442(2004)017<0294:UIPATI>2.0.CO;2.
Ferraro, R. R., N. C. Grody, and G. F. Marks (1994), Effects of surface conditions on rain identification using the DMSP-SSM/I, *Remote Sens. Rev.*, *11*(1–4), 195–209, doi:10.1080/02757259409532265.
Funk, C., et al. (2015), The climate hazards infrared precipitation with stations–a new environmental record for monitoring extremes, *Sci. Data*, doi:10.1038/sdata.2015.66.
Getirana, A. C. V., J. C. V. Espinoza, J. Ronchail, and O. C. Rotunno Filho (2011), Assessment of different precipitation datasets and their impacts on the water balance of the Negro River basin, *J. Hydrol.*, *404*(3–4), 304–322, doi:10.1016/j.jhydrol.2011.04.037.
Giannini, A., M. Biasutti, and M. M. Verstraete (2008), A climate model-based review of drought in the Sahel: Desertification, the re-greening and climate change, *Global Planet. Change*, *64*(3), 119–128, doi:10.1016/j.gloplacha.2008.05.004.
Griffies, S. M., M. J. Harrison, R. C. Pacanowski, and A. Rosati (2004), A technical guide to MOM4, GFDL Ocean Group Tech. Rep. No. 5, NOAA/Geophysical Fluid Dyn. Lab. [Available at http://www.gfdl.noaa.gov.]
Grody, N. C. (1991), Classification of snow cover and precipitation using the special sensor microwave imager, *J. Geophys. Res.*, *96*(D4), 7423–7435, doi:10.1029/91JD00045.
Hallack-Alegria, M., and D. W. Watkins (2007), Annual and warm season drought intensity–duration–frequency analysis for Sonora, Mexico, *J. Clim.*, *20*(9), 1897–1909, doi:10.1175/JCLI4101.1.
Harris, I., P. D. Jones, T. J. Osborn, and D. H. Lister (2014), Updated high-resolution grids of monthly climatic observations—The CRU TS3.10 Dataset, *Int. J. Climatol.*, *34*(3), 623–642, doi:10.1002/joc.3711.
Huffman, G. J., R. F. Adler, M. M. Morrissey, D. T. Bolvin, S. Curtis, R. Joyce, B. McGavock, and J. Susskind (2001), Global precipitation at one-degree daily resolution from multisatellite observations, *J. Hydrometeorol.*, *2*(1), 36–50, doi:10.1175/1525-7541(2001)002<0036:GPAODD>2.0.CO;2.
Huffman, G. J., D. T. Bolvin, E. J. Nelkin, D. B. Wolff, R. F. Adler, G. Gu, Y. Hong, K. P. Bowman, and E. F. Stocker (2007), The TRMM Multisatellite Precipitation Analysis (TMPA): Quasi-global, multiyear, combined-sensor precipitation estimates at fine scales, *J. Hydrometeorol.*, *8*(1), 38–55, doi:10.1175/JHM560.1.
Kalnay, E., et al. (1996), The NCEP/NCAR 40-year reanalysis project, *Bull. Am. Meteorol. Soc.*, *77*(3), 437–471, doi:10.1175/1520-0477(1996)077<0437:TNYRP>2.0.CO;2.
Kanamitsu, M. (1989), Description of the NMC global data assimilation and forecast system, *Weather Forecast.*, *4*(3), 335–342, doi:10.1175/1520-0434(1989)004<0335:DOTNGD>2.0.CO;2.
Kanamitsu, M., J. C. Alpert, K. A. Campana, P. M. Caplan, D. G. Deaven, M. Iredell, B. Katz, H.-L. Pan, J. Sela, and G. H. White (1991), Recent changes implemented into the global forecast system at NMC, *Weather Forecast.*, *6*(3), 425–435, doi:10.1175/1520-0434(1991)006<0425:RCIITG>2.0.CO;2.
Kanamitsu, M., W. Ebisuzaki, J. Woollen, S.-K. Yang, J. J. Hnilo, M. Fiorino, and G. L. Potter (2002), NCEP–DOE AMIP-II Reanalysis (R-2), *Bull. Am. Meteorol. Soc.*, *83*(11), 1631–1643, doi:10.1175/BAMS-83-11-1631.
Kasei, R., B. Diekkrüger, and C. Leemhuis (2010), Drought frequency in the Volta Basin of West Africa, *Sustainability Sci.*, *5*(1), 89–97, doi:10.1007/s11625-009-0101-5.
Kim, S., B. Kim, T. J. Ahn, and H. S. Kim (2011), Spatio-temporal characterization of Korean drought using severity-area-duration curve analysis, *Water Environ. J.*, *25*(1), 22–30, doi:10.1111/j.1747-6593.2009.00184.x.
Kistler, R., S. Saha, and J. Woollen (1994), The NMC/NCAR reanalysis monitoring system, in *Proc. 19th Annual Climate Diagnostics Workshop*, pp. 226–229, U.S. Dept. of Commerce, College Park, Md.
Koster, R. D., M. J. Suarez, A. Ducharne, M. Stieglitz, and P. Kumar (2000), A catchment-based approach to modeling land surface processes in a general circulation model: 1. Model structure, *J. Geophys. Res.*, *105*(D20), 24,809–24,822, doi:10.1029/2000JD900327.
Koutsouris, A. J., D. Chen, and S. W. Lyon (2015), Comparing global precipitation data sets in eastern Africa: A case study of Kilombero Valley, Tanzania, *Int. J. Climatol.*, *36*(4), 2000–2014, doi:10.1002/joc.4476.
Liang, X., D. P. Lettenmaier, E. F. Wood, and S. J. Burges (1994), A simple hydrologically based model of land surface water and energy fluxes for general circulation models, *J. Geophys. Res.*, *99*(D7), 14,415–14,428, doi:10.1029/94JD00483.
Liang, X., E. F. Wood, and D. P. Lettenmaier (1996), Surface soil moisture parameterization of the VIC-2 L model: Evaluation and modification, *Global Planet. Change*, *13*(1–4), 195–206, doi:10.1016/0921-8181(95)00046-1.
Lin, R., T. Zhou, and Y. Qian (2014), Evaluation of global monsoon precipitation changes based on five reanalysis datasets, *J. Clim.*, *27*(3), 1271–1289, doi:10.1175/JCLI-D-13-00215.1.
Lloyd-Hughes, B., and M. A. Saunders (2002), A drought climatology for Europe, *Int. J. Climatol.*, *22*(13), 1571–1592, doi:10.1002/joc.846.
Lorenz, C., and H. Kunstmann (2012), The Hydrological cycle in three state-of-the-art reanalyses: Intercomparison and performance analysis, *J. Hydrometeorol.*, *13*(5), 1397–1420, doi:10.1175/JHM-D-11-088.1.
Marengo, J. A. (2005), Characteristics and spatio-temporal variability of the Amazon River Basin Water Budget, *Clim. Dyn.*, *24*(1), 11–22, doi:10.1007/s00382-004-0461-6.
Masih, I., S. Maskey, F. E. F. Mussá, and P. Trambauer (2014), A review of droughts on the African continent: A geospatial and long-term perspective, *Hydrol. Earth Syst. Sci.*, *18*(9), 3635–3649, doi:10.5194/hess-18-3635-2014.
Maurer, E. P., G. M. O'Donnell, D. P. Lettenmaier, and J. O. Roads (2001), Evaluation of the land surface water budget in NCEP/NCAR and NCEP/DOE reanalyses using an off-line hydrologic model, *J. Geophys. Res.*, *106*(D16), 17,841–17,862, doi:10.1029/2000JD900828.
Mckee, T. B., N. J. Doesken, and J. Kleist (1993), The relationship of drought frequency and duration to time scales, in *AMS 8th Conference on Applied Climatology*, pp. 179–184, Anaheim, Calif.

Meng, J., R. Yang, H. Wei, M. B. Ek, G. Gayno, P. Xie, and K. Mitchell (2012), The land surface analysis in the NCEP climate forecast system reanalysis, *J. Hydrometeorol.*, *13*(5), 1621–1630, doi:10.1175/JHM-D-11-090.1.
Mintz, Y., and Y. V. Serafini (1992), A global monthly climatology of soil moisture and water balance, *Clim. Dyn.*, *8*(1), 13–27, doi:10.1007/BF00209340.
Mishra, A. K., and V. P. Singh (2009), Analysis of drought severity-area-frequency curves using a general circulation model and scenario uncertainty, *J. Geophys. Res.*, *114*, D06120, doi:10.1029/2008JD010986.
Mishra, A. K., and V. P. Singh (2010), A review of drought concepts, *J. Hydrol.*, *391*(1–2), 202–216, doi:10.1016/j.jhydrol.2010.07.012.
Mo, K. C., and M. Chelliah (2006), The modified palmer drought severity index based on the NCEP North American regional reanalysis, *J. Appl. Meteorol. Climatol.*, *45*(10), 1362–1375, doi:10.1175/JAM2402.1.
New, M., M. Hulme, and P. D. Jones (2000), Representing twentieth-century space–time climate variability. Part II: Development of 1901–96 monthly grids of terrestrial surface climate, *J. Clim.*, *13*(13), 2217–2238, doi:10.1175/1520-0442(2000)013<2217:RTCSTC>2.0.CO;2.
Nicholson, S. E. (2000), The nature of rainfall variability over Africa on time scales of decades to millenia, *Global Planet. Change*, *26*(1), 137–158, doi:10.1016/S0921-8181(00)00040-0.
Nijssen, B., R. Schnur, and D. P. Lettenmaier (2001), Global retrospective estimation of soil moisture using the variable infiltration capacity land surface model, 1980–93, *J. Clim.*, *14*(8), 1790–1808, doi:10.1175/1520-0442(2001)014<1790:GREOSM>2.0.CO;2.
Novella, N. S., and W. M. Thiaw (2013), African rainfall climatology version 2 for famine early warning systems, *J. Appl. Meteorol. Theor. Appl. Climatol.*, *52*(3), 588–606, doi:10.1175/JAMC-D-11-0238.1.
Ntale, H. K., and T. Y. Gan (2003), Drought indices and their application to East Africa, *Int. J. Climatol.*, *23*(11), 1335–1357, doi:10.1002/joc.931.
Peña-Arancibia, J. L., A. I. J. M. van Dijk, L. J. Renzullo, and M. Mulligan (2013), Evaluation of precipitation estimation accuracy in reanalyses, satellite products, and an ensemble method for regions in Australia and South and East Asia, *J. Hydrometeorol.*, *14*(4), 1323–1333, doi:10.1175/JHM-D-12-0132.1.
Poccard, I., S. Janicot, and P. Camberlin (2000), Comparison of rainfall structures between NCEP/NCAR reanalyses and observed data over tropical Africa, *Clim. Dyn.*, *16*(12), 897–915, doi:10.1007/s003820000087.
Rienecker, M. M., M. J. Suqarez, R. Todling, J. Bacmeister, L. L. Takacs, H.-C. Liu, W. Gu, and M. Scienkiewicz (2008), The GEOS-5 data assimilation system—Documentation of versions 5.0.1, 5.1.0, and 5.2.0, Greenbelt, Md.
Rienecker, M. M., et al. (2011), MERRA: NASA's modern-era retrospective analysis for research and applications, *J. Clim.*, *24*(14), 3624–3648, doi:10.1175/JCLI-D-11-00015.1.
Roads, J. O. (2003), The NCEP–NCAR, NCEP–DOE, and TRMM tropical atmosphere hydrologic cycles, *J. Hydrometeorol.*, *4*(5), 826–840, doi:10.1175/1525-7541(2003)004<0826:TNNATT>2.0.CO;2.
Rouault, M., and Y. Richard (2005), Intensity and spatial extent of droughts in southern Africa, *Geophys. Res. Lett.*, *32*, L15702, doi:10.1029/2005GL022436.
Saha, S., S. Nadiga, C. Thiaw, and J. Wang (2006), The NCEP climate forecast system, *J. Clim.*, *19*(15), 3483–3517, doi:10.1175/JCLI3812.1.
Saha, S., et al. (2010), The NCEP climate forecast system reanalysis, *Bull. Am. Meteorol. Soc.*, *91*(8), 1015–1057, doi:10.1175/2010BAMS3001.1.
Sheffield, J., and E. F. Wood (2007), Characteristics of global and regional drought, 1950–2000: Analysis of soil moisture data from off-line simulation of the terrestrial hydrologic cycle, *J. Geophys. Res.*, *112*, D17115, doi:10.1029/2006JD008288.
Sheffield, J., and E. F. Wood (2008), Global trends and variability in soil moisture and drought characteristics, 1950–2000, from observation-driven simulations of the terrestrial hydrologic cycle, *J. Clim.*, *21*(3), 432–458, doi:10.1175/2007JCLI1822.1.
Sheffield, J., G. Goteti, F. Wen, and E. F. Wood (2004), A simulated soil moisture based drought analysis for the United States, *J. Geophys. Res.*, *109*, D24108, doi:10.1029/2004JD005182.
Sheffield, J., G. Goteti, and E. F. Wood (2006), Development of a 50-year high-resolution global dataset of meteorological forcings for land surface modeling, *J. Clim.*, *19*(13), 3088–3111, doi:10.1175/JCLI3790.1.
Sheffield, J., K. M. Andreadis, E. F. Wood, and D. P. Lettenmaier (2009), Global and continental drought in the second half of the twentieth century: Severity–area–duration analysis and temporal variability of large-scale events, *J. Clim.*, *22*(8), 1962–1981, doi:10.1175/2008JCLI2722.1.
Sheffield, J., E. F. Wood, and M. L. Roderick (2012), Little change in global drought over the past 60 years, *Nature*, *491*(7424), 435–438, doi:10.1038/nature11575.
Sheffield, J., et al. (2014), A drought monitoring and forecasting system for sub-Sahara African water resources and food security, *Bull. Am. Meteorol. Soc.*, *95*(6), 861–882, doi:10.1175/BAMS-D-12-00124.1.
Solman, S. A., et al. (2013), Evaluation of an ensemble of regional climate model simulations over South America driven by the ERA-Interim reanalysis: Model performance and uncertainties, *Clim. Dyn.*, *41*(5–6), 1139–1157, doi:10.1007/s00382-013-1667-2.
Spencer, R. W. (1993), Global oceanic precipitation from the MSU during 1979–91 and comparisons to other climatologies, *J. Clim.*, *6*(7), 1301–1326, doi:10.1175/1520-0442(1993)006<1301:GOPFTM>2.0.CO;2.
Tierney, J. E., J. E. Smerdon, K. J. Anchukaitis, and R. Seager (2013), Multidecadal variability in East African hydroclimate controlled by the Indian Ocean, *Nature*, *493*(7432), 389–392, doi:10.1038/nature11785.
United Nations Office for the Coordination of Humanitarian Affairs (2011), Horn of Africa drought crisis situation report NO. 5 Published on ReliefWeb. [Available at http://reliefweb.int/sites/reliefweb.int/files/resources/Full_report_170.pdf, Accessed April 14, 2016.]
Vicente-Serrano, S. M., et al. (2012), Challenges for drought mitigation in Africa: The potential use of geospatial data and drought information systems, *Appl. Geogr.*, *34*, 471–486, doi:10.1016/j.apgeog.2012.02.001.
Vidal, J.-P., E. Martin, L. Franchistéguy, F. Habets, J.-M. Soubeyroux, M. Blanchard, and M. Baillon (2009), Multilevel and multiscale drought reanalysis over France with the Safran-Isba-Modcou hydrometeorological suite, *Hydrol. Earth Syst. Sci. Discuss.*, *6*(5), 6455–6501, doi:10.5194/hessd-6-6455-2009.
Vidal, J. P., E. Martin, L. Franchistéguy, F. Habets, J. M. Soubeyroux, M. Blanchard, and M. Baillon (2010), Multilevel and multiscale drought reanalysis over France with the Safran-Isba-Modcou hydrometeorological suite, *Hydrol. Earth Syst. Sci. Discuss.*, *14*(3), 459–478, doi:10.5194/hess-14-459-2010.
Wang, A., T. J. Bohn, S. P. Mahanama, R. D. Koster, and D. P. Lettenmaier (2009), Multimodel ensemble reconstruction of drought over the continental United States, *J. Clim.*, *22*(10), 2694–2712, doi:10.1175/2008JCLI2586.1.
Wang, A., D. P. Lettenmaier, and J. Sheffield (2011), Soil moisture drought in China, 1950–2006, *J. Clim.*, *24*(13), 3257–3271, doi:10.1175/2011JCLI3733.1.
Whitaker, J. S., G. P. Compo, X. Wei, and T. M. Hamill (2004), Reanalysis without radiosondes using ensemble data assimilation, *Mon. Weather Rev.*, *132*(5), 1190–1200, doi:10.1175/1520-0493(2004)132<1190:RWRUED>2.0.CO;2.
Wilheit, T. T., A. T. C. Chang, and L. S. Chiu (1991), Retrieval of monthly rainfall indices from microwave radiometric measurements using probability distribution functions, *J. Atmos. Oceanic Technol.*, *8*(1), 118–136, doi:10.1175/1520-0426(1991)008<0118:ROMRIF>2.0.CO;2.

Wu, W.-S., R. J. Purser, and D. F. Parrish (2002), Three-dimensional variational analysis with spatially inhomogeneous covariances, *Mon. Weather Rev.*, *130*(12), 2905–2916, doi:10.1175/1520-0493(2002)130<2905:TDVAWS>2.0.CO;2.

Xie, P., and P. A. Arkin (1995), An intercomparison of gauge observations and satellite estimates of monthly precipitation, *J. Appl. Meteorol.*, *34*(5), 1143–1160, doi:10.1175/1520-0450(1995)034<1143:AIOGOA>2.0.CO;2.

Xie, P., and P. A. Arkin (1997), Global precipitation: A 17-year monthly analysis based on gauge observations, satellite estimates, and numerical model outputs, *Bull. Am. Meteorol. Soc.*, *78*(11), 2539–2558, doi:10.1175/1520-0477(1997)078<2539:GPAYMA>2.0.CO;2.

Xie, P., M. Chen, S. Yang, A. Yatagai, T. Hayasaka, Y. Fukushima, and C. Liu (2007), A gauge-based analysis of daily precipitation over East Asia, *J. Hydrometeorol.*, *8*(3), 607–626, doi:10.1175/JHM583.1.

Zhang, L., A. Kumar, and W. Wang (2012), Influence of changes in observations on precipitation: A case study for the Climate Forecast System Reanalysis (CFSR), *J. Geophys. Res.*, *117*, D08105, doi:10.1029/2011JD017347.

Zhang, Q., H. Körnich, and K. Holmgren (2013), How well do reanalyses represent the southern African precipitation?, *Clim. Dyn.*, *40*(3–4), 951–962, doi:10.1007/s00382-012-1423-z.